University of Szeged

Faculty of Pharmacy

Institute of Pharmaceutical Technology and Regulatory Affairs

Head: Prof. Dr. Ildikó Csóka, Pharm.D., Ph.D.

Ph.D. Thesis

Improving the absorption of poorly permeable drugs through alternative delivery routes using nanocarriers

By

Maryana Yahia Salamah

Pharm.D., M.Sc.

Supervisors:

Prof. Dr. György Tibor Balogh D.Sc.

Dr. habil. Gábor Katona, Ph.D.

Szeged
2025

PUBLICATIONS RELATED TO THE THESIS:

- **Salamah, M.;** Volk, B.; Lekli, I.; Bak, I.; Gyöngyösi, A.; Kozma, G.; Kónya, Z.; Szalenkó-Tőkés, Á.; Kiricsi, Á.; Rovó, L.; Balogh-Weiser, D., Zupkó, I., Csóka, I., Katona, G., Balogh, G.T. Preparation, and Ex Vivo and in Vivo Characterization of Favipiravir-Loaded Aspasomes and Niosomes for Nose-to-Brain Administration. Int J Nanomedicine 2025, 20, 6489–6514, doi:10.2147/IJN.S518486.
  (D1, IF: 6.5).
- **Salamah, M.;** Sipos, B.; Schelz, Z.; Zupkó, I.; Kiricsi, Á.; Szalenkó-Tőkés, Á.; Rovó, L.; Katona, G.; Balogh, G.T.; Csóka, I. Development, in Vitro and Ex Vivo Characterization of Lamotrigine-Loaded Bovine Serum Albumin Nanoparticles Using QbD Approach. Drug Deliv 2025, 32, doi:10.1080/10717544.2025.2460693.
  (D1, IF: 6.5).

PUBLICATIONS NOT RELATED TO THE THESIS:

- **Salamah, M.;** Sipos, B.; Katona, G.; Volk, B.; Balogh, G.T.; Csóka, I. Development and Validation of a Novel Isocratic RP-HPLC Method Using AQbD Approach for the Quantification of Favipiravir. European Journal of Pharmaceutical Sciences 2025, 214, 107276, doi:10.1016/J.EJPS.2025.107276.
  (Q1, IF: 4.7).
- **Salamah, M.;** Budai-Szűcs M.; Sipos, B.; Volk, B.; Katona, G.; Tibor Balogh, G.; Csóka, I. Development and Characterization of In Situ Gelling Nasal Cilostazol Spanlastics. Gels 2025, Vol. 11, Page 82 2025, 11, 82, doi:10.3390/GELS11020082.
  (Q1, IF: 5.3).
- Balogh-Weiser, D.; Molnár, A.; Tóth, G. D.; Koplányi, G.; Szemes, J.; Decsi, B.; Katona, G.; **Salamah, M.;** Ender, F.; Kovács, A.; Berkó, S.; Budai-Szűcs, M.; Balogh, G. T. Combined Nanofibrous Face Mask: Co-Formulation of Lipases and Antibiotic Agent by Electrospinning Technique. Pharmaceutics 2023, 15 (4), 1174. https://doi.org/10.3390/pharmaceutics15041174.
  (Q1, IF: 4.9).

PRESENTATIONS RELATED TO THE SUBJECT OF THE THESIS

A. Oral presentations

1) **Salamah, M.;** Balogh, G.T.; Katona, G. (2022). Improving the bioavailability of Favipiravir by using human serum albumin nanoparticles. IV. Symposium of Young Researchers on Pharmaceutical Technology, Biotechnology and Regulatory Science, Szeged, Hungary.
2) **Salamah, M.;** Balogh, G.T.; Katona, G. (2023). Formulation and Optimization of Lamotrigine-Loaded Bovine Serum Albumin Nanoparticles by Using Full Factorial Design. V. Symposium of Young Researchers on Pharmaceutical Technology, Biotechnology and Regulatory Science, Szeged, Hungary.
3) **Salamah, M.;** Balogh, G.T.; Katona, G. (2023). Preparation, *in vitro* and *ex vivo* evaluation of favipiravir loaded niosomes for nose-to-brain administration. Medicinal Chemistry and Pharmaceutical Technology Symposium '23, Herceghalom, Hungary.
4) **Salamah, M.;** G.; Katona, G. (2023). Quality by Design Approach for Optimization of Lamotrigine-Loaded Bovine Serum Albumin Nanoparticles for Intranasal Administration. XV. Ottó Clauder Memorial Competition, Budapest, Hungary.
5) **Salamah, M.;** Balogh, G.T.; Katona, G. (2024). Formulation and optimization of rifampicin-loaded niosomes for ocular delivery system. VI. Symposium of Young Researchers on Pharmaceutical Technology, Biotechnology and Regulatory Science, Szeged, Hungary.
6) Katona, G.; **Salamah, M.;** Sipos, B.; Schelz, Z.; Zupkó, I.; Balogh, G.T.; Csóka, I. (2024). Investigation of the Effect of Different Cross-Linking Agents on the Colloidal Properties of Albumin Nanoparticles. Congressus Pharmaceuticus Hungaricus XVII. and EUFEPS Annual Meeting, Debrecen, Hungary.
7) **Salamah, M.;** Balogh, G.T.; Katona, G. (2024). Rifampicin-loaded niosomes: optimization, *in vitro* and *ex vivo* characterization. XXVII. Spring Wind Conference, Budapest, Hungary.
8) **Salamah, M.;** Volk, B.; Csóka, I.; Balogh, G.T.; Katona, G. (2024). Novel mucoadhesion chitosomes for nose-to-brain delivery of favipiravir. 7th Young Technologists' Forum, Budapest, Hungary.
9) **Salamah, M.;** Budai-Szűcs M.; Sipos, B.; Volk, B.; Katona, G.; Tibor Balogh, G.; Csóka, I. (2025). Cilostazol spanlastic vesicles-loaded in situ gel for nose-to-brain delivery system. VII. Symposium of Young Researchers on Pharmaceutical Technology, Biotechnology and Regulatory Science, Szeged, Hungary.
10) **Salamah, M.;** Balogh, G.T.; Katona, G. (2025). Rifampicin-loaded lipidic liquid-crystalline phases (cubosomes) for nose-to-brain delivery system for CNS tuberculosis. 8th Young Technologists' Forum, Budapest, Hungary.

B. Poster presentations

1) **Salamah, M.;** Balogh, G.T.; Katona, G. (2023). Preparation, *In Vitro* and *Ex Vivo* Characterization of Lamotrigine-Loaded Bovine Serum Albumin Nanoparticles Using QbD Approach. European Federation for Pharmaceutical Sciences (EUFEPS) Annual meeting, Lisbon, Portugal.
2) **Salamah, M.;** Balogh, G.T.; Katona, G. (2025). Doxorubicin-loaded cubosomes functionalized with hyaluronic acid for intranasal administration. 1st International Health Science Conference Szeged, Szeged, Hungary.
3) **Salamah, M.;** Volk, B.; Lekli, I.; Bak, I.; Gyöngyösi, A.; Csóka, I.; Balogh, G.T.; Katona, G. (2025). Evaluation of *in vivo* nose-to-brain delivery of favipiravir-loaded aspasomes. 15th Central European Symposium on Pharmaceutical Technology, Bled, Slovenia**.**

ABBREVIATIONS

Abbreviation	Description
AEDs	Antiepileptic drugs
AIC	Akaike information criterion
ANOVA	Analysis of variance
AP	Ascorbyl palmitate
ASPs	Aspasomes
AUC	Area under the curve
AVDs	Antiviral drugs
BBB	Blood-brain-barrier
BBB-PAMPA	Blood-brain barrier-specific parallel artificial membrane permeability assay
BCS	Biopharmaceutics classification system
BCSFB	Blood-cerebrospinal fluid barrier
BSA	Bovine serum albumin
$CaCl_2$	Calcium chloride
Caco-2	Human colon adenocarcinoma
CH	Cholesterol
CL	Clearance
Cmax	Maximum concentration
CNS	Central nervous system
COX-2	Cyclooxygenase-2
CSF	Cerebrospinal fluid
DE	Dissolution efficiency
DL	Drug loading
DMSO	Dimethyl sulfoxide
DoE	Design of Experiments
DPBS	Dulbecco's phosphate-buffered saline
EDC	1-(3-dimethylaminutesopropyl)-3-ethylcarbodiimide hydrochloride
EE	Encapsulation efficiency
ER	Enhancement ratio
EtOH	Ethanol
F%	Relative bioavailability
FAV	Favipiravir
FAV-ASP	Favipiravir-loaded aspasomes
FESS	Functional endoscopic sinus surgery
GC-MS	Gas chromatograph-mass spectrometric
HLB	Hydrophilic-lipophilic balance
HPLC	High-performance liquid chromatography
HSA	Human serum albumin
IN	Intranasal
IV	Intravenous
IVIVC	In vitro-in vivo correlations
J_{ss}	Steady-state flux

K	Release rate constant
KCl	Potassium chloride
k_e	Elimination rate constant
K_p	Permeability coefficient
LAM	Lamotrigine
LAM-BSA	Lamotrigine-loaded bovine serum albumin nanoparticles
LOD	Limit of detection
LOQ	Limit of quantification
MDT	Mean dissolution time
MeOH	Methanol
MRT	Mean residence time
MSC	Model selection criterion
NaCl	Sodium chloride
NMDA	N-methyl-d-aspartate
NPs	Nanoparticles
Papp	Apparent permeability coefficients
PDI	Polydispersity index
PGE2	Prostaglandin E2
P-gp	P-glycoprotein
PK	Pharmacokinetic
PNS	Peripheral nervous system
R^2	Correlation coefficient
RED	Rapid equilibrium dialysis
SARS-CoV-2	Severe acute respiratory syndrome coronavirus 2
SD	Standard deviation
SNES	Simulated nasal electrolyte solution
$t_{1/2}$	Elimination half-life
T-705RTP	Favipiravir ribofuranosyl-5'-triphosphate
TEER	Transepithelial electric resistance
UGT	Uridine-diphosphate glucuronosyltransferase
US-FDA	United States-Food and Drug Administration
V_d	Volume of distribution
WHO	World health organization
Z-average	Average hydrodynamic diameter
ZP	Zeta potential

TABLE OF CONTENTS

1. Introduction

The increasing prevalence and severity of central nervous system (CNS) disorders pose a serious, life-threatening condition, which could cause lifelong disability or could be associated with sudden death. CNS disorders include acute brain injury and cerebrovascular diseases (such as stroke, cerebral ischemia, and epilepsy), and neurodegenerative diseases (such as Alzheimer's, Parkinson's, and Huntington's diseases) [1,2].

The drug discovery for CNS disorders is a long-term, expensive process with a low success rate in clinical trials, which is associated with the physiological barriers that impede drug permeation, including the blood-brain-barrier (BBB) and blood-cerebrospinal fluid barrier (BCSFB) [3,4]. Therefore, the pharmaceutical research has been focused on improving the BBB permeability of the marketed drugs by developing suitable drug carriers and using alternative routes of administration [5]. The BBB comprises continuous cerebrovascular endothelial cells and their intercellular tight junctions, intact basement membranes, pericytes, and membranes surrounded by astrocyte foot plates. On the other hand, the BCSFB consists of the brain endothelial cells, choroid plexus epithelial cells, and the arachnoid membrane, which envelops the brain [6].

In recent decades, intranasal (IN) administration has emerged in pharmaceutical research as a promising non-invasive strategy for targeted drug delivery to the brain, via the olfactory nerve pathway, olfactory mucosal epithelial pathway, trigeminal nerve pathway, and blood circulation pathway [7,8].

IN administration requires selecting an appropriate drug delivery system to overcome the physiological barriers in both nasal cavity (such as mucus barrier, mechanism of mucociliary clearance, enzymatic activity and tight junctions in the olfactory epithelium), and the brain (such as tight junctions in BBB, pericytes and astrocytes, efflux transporters and metabolic enzymes) which limit the permeation of ~ 98% of the drugs [9–11]. Therefore, the physicochemical properties of the drug delivery system, including lipophilicity, biodegradability, particle size, surface charge, and mucoadhesion properties, have a crucial role in facilitating effective drug absorption and distribution of the drug from the nasal cavity to the brain [12,13]. Accordingly, nanoparticles provide a promising drug delivery for CNS targeting and overcome the limits of conventional pharmaceutical formulations.

Nanoparticles (NPs) have been used in many studies for nose-to-brain delivery system due to their advantages, including promoting drug accumulation in the CNS through an increased permeation across the olfactory region, protecting the drug from enzymatic degradation, and prolonging nasal residence time [14].

Several types of nanoparticles, including lipid-based formulations such as liposomes, niosomes, and aspasomes, as well as albumin-based nanoparticles like bovine serum albumin (BSA) nanoparticles, have been developed to enhance the delivery of drugs to the CNS, depending on their surface area, surface charge, solubility, viscosity and biodegradability [15,16].

2. Aim of the work

This Ph.D. work aimed to develop and characterize two novel nanocarrier systems for possible nose-to-brain delivery of lamotrigine and favipiravir (lamotrigine-loaded bovine serum albumin nanoparticles and favipiravir-loaded aspasomes) as poorly permeable model CNS active drugs intended for the treatment of epilepsy and neurotropic RNA virus infections.

This Ph.D. work was designed and studied according to the following steps:

- ✓ Performing a systematic literary review about epilepsy and CNS viral infection, as well as lipid and albumin nanoparticles as suitable nano-drug delivery systems for nose-to-brain delivery.
- ✓ Determining the factors which could influence the preparation of lamotrigine-loaded bovine serum albumin nanoparticles and use full factorial design for the optimization.
- ✓ Determining the factors which could influence the preparation of favipiravir-loaded aspasomes.
- ✓ Performing *in vitro* evaluation of both optimized nanocarriers, regarding to physical and chemical properties, and nasal applicability.
- ✓ Conducting *in vitro* cell line studies to evaluate the cytotoxicity and cell permeability of lamotrigine-loaded bovine serum albumin nanoparticles.
- ✓ Carrying out *ex vivo* studies using human nasal mucosa to predict the permeability through the nasal epithelium for both optimized nanocarriers.
- ✓ Performing *in vivo* studies to evaluate the bioavailability of favipiravir-loaded aspasomes in plasma and CSF samples.
- ✓ Finally, assessing the storage stability of favipiravir-loaded aspasomes.

3. Literature background of the research work

3.1. Epilepsy and CNS viral infection

Epilepsy, the second common CNS disorder caused by abnormal electrical activity in the brain, affects around 50 million people globally, according to the World Health Organization (WHO) [17], and is characterized by recurrent unprovoked epileptic seizures [18]. Seizures occur due to abnormal excitement and a lack of inhibition in the neural networks of CNS. Most of the seizures usually stopped after 5 minutes without immediate treatment. However, if the seizures last for more than 5-10 minutes, then it is difficult to stop and control without treatment. On the other hand, recurrent seizures for 30 minutes could cause disability or be associated with the risk of premature death, depending on the duration of the seizures [19,20]. Children have a higher incidence of epilepsy compared to adult patients [21].

There are several causes of epilepsy, including traumatic brain injury, cerebrovascular accidents, tumours, viral and bacterial infection of CNS, and genetic causes [22]. Seizures could indicate other disorders, such as infection and metabolic imbalance, or reflect deterioration or alteration of underlying neurological disorders [23,24]. Seizures are a primary symptom of viral infections of the CNS, which could occur during the infection or after recovery and result in acquired epilepsy [25]. In many cases, the CNS viral infections remain undiagnosed, which significantly contributes to increased morbidity and mortality in adults and neonates [26,27]. Several viruses, especially neurotropic RNA viruses (such as poliovirus, Zika virus, influenza A and B, and severe acute respiratory syndrome coronavirus 2 (SARS-CoV-2)), are contributing in the development of seizures and epilepsy by the disrupting in the integrity of BBB and BCSFB following invasion of the brain through the nasal epithelium, or the choroid plexus into the CSF, or the pseudounipolar sensory neurons of the peripheral nervous system (PNS) [25,28].

Disruption in the BBB is associated with the onset and progression of neurodegenerative disorders, epilepsy, and metabolic diseases, or the seizures themselves may impair BBB integrity by activation of astrocytes and innate immunological responses, tight junction aberration, pericyte-microglia clustering and a thickening of the capillary basement membrane [29,30]. Furthermore, the elevated in brain glutamate levels induced by seizures leads to activation of *N*-methyl-D-aspartate (NMDA) receptor and cyclooxygenase-2 (COX-2) in brain capillaries, which then, via prostaglandin E2 (PGE2) receptors, increases the expression of multidrug efflux transporters in astrocyte end-feet, as a second line defence, including P-glycoprotein (P-gp), which could cause pharmaco-resistance to antiepileptic and antiviral drugs [31,32]. Therefore, it is critical to develop suitable drug carriers along with alternate routes of administration.

3.1.1. Antiepileptic drugs (AEDs): Lamotrigine (LAM)

Antiepileptic drugs (AEDs) act by selectively modifying the excitability of neurons, resulting in inhibition of seizure-specific neuronal firing without affecting normal signals; therefore, AEDs could manage seizures but do not cure epilepsy [33]. To ensure effective treatment, AEDs should reach the CNS at therapeutic concentrations with minimal adverse effects. Among AEDs, lamotrigine (LAM) has shown good efficiency in reducing seizure frequency with fewer adverse side effects [22,33].

LAM is a second-generation antiepileptic and mood stabilizing drug, which belongs to Biopharmaceutics Classification System (BCS) class II drug (low water solubility ~ 0.17 mg/mL) [34]. It was approved by the United States-Food and Drug Administration (FDA) and recommended by international guidelines and the neurological disorder association for the treatment of epilepsy with an initial oral dose of 25 mg daily for two weeks, followed by an increase to 50 mg daily for two weeks, and subsequently, a further 50 mg should be administered each week or every other week [35,36]. LAM selectivity binds and inhibits both sodium and N- and L-type calcium channels, stabilizing presynaptic neuronal membranes and inhibiting presynaptic glutamate and aspartate release. It is used as monotherapy or combination therapy for the treatment of partial seizures in adults, primary generalized tonic-clonic seizures, and generalized seizures in children and adults, as well as bipolar I disorder [36–38]. Moreover, LAM is indicated for conversion from an enzyme-inducing AEDs (such as carbamazepine and phenobarbital) or valproate to monotherapy in adults with partial seizures [39]. Furthermore, LAM was reported as the first-line management of neuropathic pain and trigeminal neuralgia [40].

LAM undergoes first-pass hepatic metabolism via glucuronidation using uridine-diphosphate glucuronosyltransferase (UGT) enzymes, and is excreted renally, with an elimination half-life of 24-37 hours. As reported in the literature, LAM is safe at therapeutic concentrations of 2.5 to 15 mg/L and shows dose-dependent toxicity at concentrations above 20 mg/L [39]. Furthermore, LAM is a substrate of P-gp, which may explain its restricted access to the brain because the overexpression of P-gp in BBB; therefore, a higher dose of LAM is required to achieve a therapeutic concentration. However, this could be associated with increased adverse effects, including hepatotoxicity, thrombocytopenia, headache, dizziness, sedation, and Stevens-Johnson syndrome [16,41].

Currently, LAM is available in tablet dosage form for oral administration. However, the oral bioavailability of LAM is low due to the low solubility, extensive first-pass hepatic metabolism, and limited permeability across BBB and BCSFB, resulting in low therapeutic efficacy.

Consequently, novel drug delivery systems and alternative routes of administration are required to overcome the bioavailability obstacles.

3.1.2. Antiviral drugs (AVDs): Favipiravir (FAV)

Antiviral drugs (AVDs) exhibit different mechanisms of action, including targeting the host cell or direct targeting of the viruses (inhibitors of virus attachment or entry, polymerase inhibitors, protease inhibitors, inhibitors of nucleoside and nucleotide reverse transcriptase) [42]. Some AVDs are prodrugs, which require intracellular enzymatic conversion into their active metabolite to achieve their therapeutic effect; therefore, these AVDs should cross the brain cellular membrane to inhibit these viruses inside the brain cells [43]. On the other hand, to ensure effective treatment for viral CNS infections, AVDs should bypass BBB and BCSFB to reach the brain at sufficient concentrations with minimal adverse effects. However, few clinically approved AVDs in the market for systemic indications have demonstrated efficacy for viral CNS infections [26,43]. Among AVDs, favipiravir (FAV, T-705) has emerged as a potential candidate for the treatment of RNA virus infections, including Influenza, Ebola, Zika viruses, and SARS-CoV-2 [44]. FAV is an antiviral prodrug, belongs to BCS class II drug (low water solubility ~ 8.7 µg/mL). It was approved by FDA for the treatment of new-onset or recurrent pandemic influenza and recommended by the clinical trials for emergency use against SARS-CoV-2 [45,46]. Based on the literature, FAV has been considered as a drug of choice for SARS-CoV-2 in the newborn for short-term use [47].

It is available in an oral solid dosage form, with a recommended dosage of 1600 mg twice daily on day 1, followed by 600 mg twice daily on days 2 to 5 for the treatment of influenza infection, which leads to increased risk of the adverse effects, including hyperuricemia, diarrhea, increase in transaminase level [44,48]. FAV undergoes ribosylation and phosphorylation intracellularly to become in the active form favipiravir ribofuranosyl-5'-triphosphate (T-705RTP), which selectively inhibits RNA-dependent RNA polymerase of RNA viruses by incorporation into the nascent viral RNA, and this leads to inhibiting the viral replication [48].

FAV undergoes enzymatic metabolism via aldehyde oxidase/ xanthine oxidase enzymes to a hydrophilic and inactive metabolite T-705M1 and is excreted renally with an elimination half-life of 2.5-5 hours [49,50]. Based on the clinical trials, FAV could be safe and well-tolerated for short-term use [51]. FAV has a low brain permeability, which could be attributed to the low passive permeability due to its three H-bonding donors [15]. Therefore, novel drug delivery systems and alternative routes of administration are necessary to enhance its bioavailability and achieve therapeutic effects.

3.2. Nose-to-brain delivery system

The CNS is isolated from the systemic circulation primarily by the BBB and BCSFB. These barriers restrict drug transport into the CNS following oral or systemic administration; thus, higher drug doses are required to achieve a therapeutic level in the brain, which could be associated with an increased risk of adverse effects. Therefore, drug delivery approaches are necessary to overcome these barriers and improve drug bioavailability in the CNS.

Nose-to-brain delivery system is one of the most effective approaches for transporting drugs to the brain through the nasal cavity, potentially providing a faster and more targeted therapeutic effect for the treatment of CNS viral infections and epilepsy. Another challenge in the treatment of epilepsy is to find a proper route of administration to stop the seizures. Emergency treatment in epilepsy patients is generally administered orally or intravenously, if the patient can swallow during the seizure or if a medically-trained person is available to inject intravenously. Therefore, intranasal emergency treatment could be an option to ease the administration, especially in a non-medical setting at home and thereby accelerate treatment [20].

In 2019, FDA approved a commercial nasal spray of midazolam (NAYZILAM®) for patients ≥ 12 years old, and in 2020, also approved a commercial nasal spray of vitamin E solution–based diazepam nose spray (VALTOCO®) for patients ≥ 6 years old [52]. Additionally, in 2024, FDA approved the first Influenza vaccine for self-administration by intranasal delivery (FluMist®), for patients aged 2 - 49 years [53].

The nasal cavity is divided into three main regions, including the vestibular, respiratory, and olfactory region. The vestibular region is located in the anterior part of the nasal cavity and characterized by anatomical features that limit drug permeability, resulting in restricted drug absorption and permeation [54].

The respiratory region, located in the inner part of the nasal cavity, contains trigeminal nerve branches and a high-density microvasculature (which is about 5-fold higher in the respiratory region than in the olfactory region). The trigeminal nerve branches supply both the respiratory and olfactory areas and transport the drugs by intracellular transport across axons and extracellular transport via diffusion and bulk flow through perineuronal channels, perivascular spaces, or lymphatic channels connected to the CSF and brain tissues. In addition, the high-density microvasculature is partly responsible for systemic drug absorption and distribution; however, this pathway may require crossing the BBB and BCSFB, which may restrict the penetration of some drugs into the brain (as presented in Figure 1) [14,55].

Finally, the olfactory region is located at the top of the nasal cavity, below the cribriform plate, which contains olfactory cells (bipolar neurons). The drugs are transported via the olfactory nerves (along axons and through nerve bundles that cross the cribriform plate), eventually reaching the olfactory bulb and then to deeper areas of the brain [7,55]. In addition, the interstitial fluid surrounding the olfactory nerve bundle is connected to the CSF in the subarachnoid space [14,54]. Therefore, as reported in the literature, the olfactory area provides a direct access to the brain through the olfactory and trigeminal nerves, while the respiratory area provides a direct pathway via trigeminal nerves, and indirect pathway via the high-density microvasculature [7,56].

Researchers have committed increased attention to the olfactory pathway after studies demonstrated that SARS-CoV-2 specifically invades the sustentacular cells and olfactory neurons in the olfactory epithelium; thus, the viral RNA and antigens could be transported to the brain through the olfactory bulb [57].

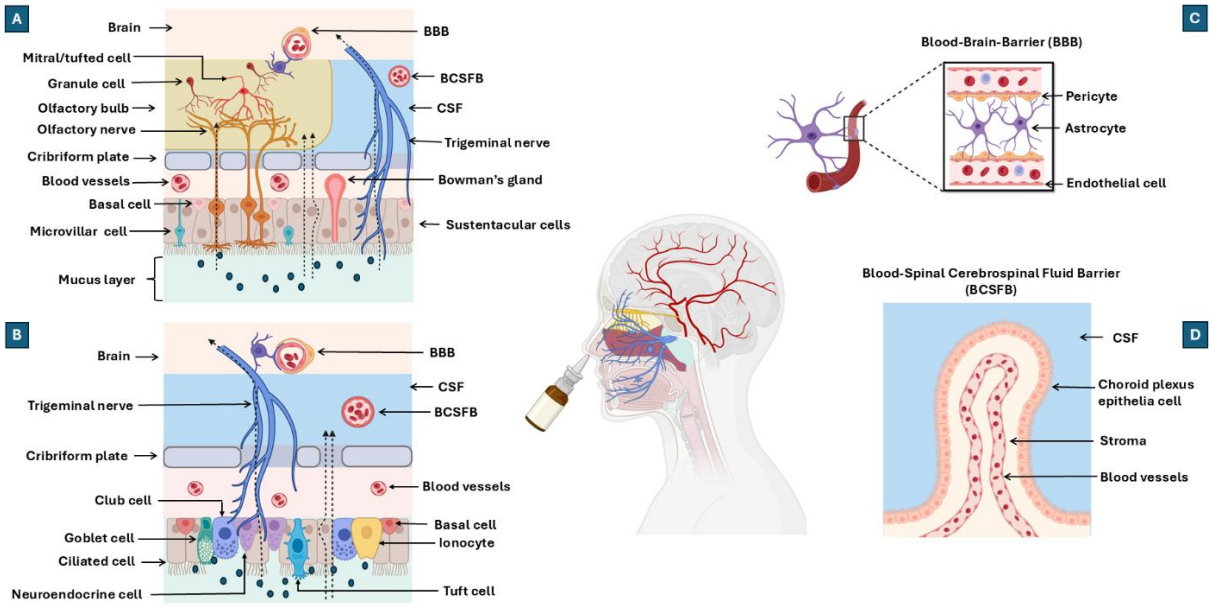

Figure 1. Schematic diagram of the physiological pathways for the nose-to-brain delivery system. The olfactory pathway (A), the respiratory pathway (B), the systemic pathway through the BBB (C), and through BCSFB (D).

Accordingly, IN administration, as a non-invasive route, offers many advantages, including ease of administration and patient compliance. It provides direct delivery of drugs to the brain via olfactory and trigeminal pathway, thereby bypassing the BBB and BCSFB, avoiding hepatic metabolism, drug degradation in the gastrointestinal tract, and reducing systemic adverse effects. Moreover, IN administration provides indirect delivery by passage across the BBB and BCSFB from the systemic

circulation [58,59]. The research demonstrated that IN administration resulted in higher, longer-lasting brain drug concentrations in comparison to intravenous (IV) administration [60].

However, because of the anatomical features and limited volume of the nasal cavity (generally around 25 to 200 µL through the olfactory epithelium [61]), high amount of doses cannot be given through IN route. Moreover, drug permeability is a challenge for hydrophilic drugs and large molecules such as peptides and proteins. Additionally, the protective mechanisms like mucociliary clearance activity, mucus barrier, enzymatic activity (such as peptidases and proteases) and tight junctions in the olfactory epithelium, reduce the retention time of drugs in the nasal cavity, leading to rapid drug removal typically within 15 minutes; especially for particles over 15 µm in size are removed [59,61,62]. Therefore, these challenges should be addressed when developing formulations for the treatment of CNS viral infections and epilepsy. Factors affecting the nasal drug absorption were summarized in Table 1.

Table 1. Factors affecting the nasal drug absorption [22,63–65]

Nasal physiology	• Mucociliary clearance • Enzymatic activity • Mucus flow • Blood flow • pH of nasal cavity • Transport and efflux systems • Pathological conditions • Environmental factors • Site of drug deposition and distribution in the nasal mucosa
Physicochemical properties of the drug	• Molecular weight • Solubility • Lipophilicity • Particle size • Surface charge. • Polymorphism and amorphism • Stability • Dissociation and partition coefficients
Physicochemical properties of the formulation	• Drug concentration • pH and mucosal irritancy • Osmolarity • Viscosity • Volume of administration • Dosage form • Excipients
Properties of the delivery device	• Type of delivery device • Droplet size distribution • Pattern of deposition

3.3. Nanoparticles for nose-to-brain delivery system

The conventional dosage forms for treating CNS disorders, including tablets, capsules, and injections, have several bioavailability challenges, such as low solubility, poor absorption, physiological barriers, first-pass metabolism, and dose-dependent toxicity. Therefore, novel drug carriers and alternative routes of administration are required to overcome these obstacles, enhance the bioavailability and achieve therapeutic effects [66].

Recently, nanoparticles (NPs) have been used as promising drug carriers to address these challenges. NPs are defined as solid colloidal particles ranging in size from 10 to 1000 nm with good biodegradability and biocompatibility properties. NPs can encapsulate and load both hydrophilic and lipophilic drugs, protecting them from enzymatic degradation and improving their stability. This provides targeted therapeutics with fewer side effects [61,67].

The physicochemical properties of the nanocarrier are a critical factor influencing the CNS targeting and therapeutic effect, which includes particle size, particle shape, surface charge, lipophilicity and pH. These properties influence the solubility, neuronal uptake, permeability across the BBB and BCSFB, release, and control drug accumulation and stability [68].

NPs have been used in many studies for nose-to-brain delivery system using biodegradable carriers, such as albumin [69,70], polymers [71], lipids [72], liposomes [73], niosomes [74] and aspasomes [15]. These biodegradable carriers impact the drug release and its pharmacokinetics and reduce the side effects. In this research, we selected aspasomes, as a lipid nanocarrier, and bovine serum albumin nanoparticles as drug carriers for antiviral drug (FAV) and antiepileptic drug (LAM), respectively.

Lipid nanoparticles, such as liposomes, niosomes and aspasomes, are considered a suitable antiviral drug carrier to enhance the BBB penetration, since the endothelial cells in the BBB are highly lipophilic [75]. This nanocarrier can protect the drug against enzymatic degradation, and improve its bioavailability, hence, prevent viral spread [15,58]. Aspasomes (ascorbyl palmitate-based nanocarriers; ASPs), a newer generation of liposomes, are composed of ascorbyl palmitate (AP) combined with cholesterol (CH) and an anionic or nonionic surfactant in various molar ratios. AP is an ester form of ascorbic acid and amphiphilic by nature, which makes ASPs able to entrap both hydrophilic and hydrophobic drug molecules [76–80]. Additionally, AP can bypass phospholipid bilayers of membranes and enter the brain through the olfactory nerves, which makes it suitable for nose-to-brain delivery systems.

Furthermore, albumin nanoparticles have been utilized as a drug carrier due to their ability to cross the BBB, improve the efficacy, pharmacokinetics and in vivo stability [81]. Among various

albumins such as human serum albumin (HSA), bovine serum albumin (BSA), and egg-white albumin (ovalbumin), BSA has been widely used in the pharmaceutical industry because of its ready availability, high purity, water solubility, low cost, non-toxic, non-immunogenic, biodegradable, and biocompatible nature [82,83]. The studies have demonstrated that BSA nanoparticles are a suitable technique to overcome the pharmaco-resistance to antiepileptic drugs, which is induced by P-gp [84,85]. Additionally, BSA is suitable for nose-to-brain delivery systems because its rapid absorption from the nasal mucosa into the brain within five minutes after IN administration via transcytosis across the nasal epithelium, followed by paracellular transport to reach deeper brain regions [86].

4. Materials

LAM (6-(2,3-dichlorophenyl)-1,2,4-triazine-3,5-diaminutese), was purchased from Teva Ltd. (Budapest, Hungary). BSA cell culture grade, ethanol (EtOH) (96% v/v), methanol (MeOH) 99.99 % v/v (HPLC grade), dimethyl sulfoxide (DMSO), mannitol, sodium chloride for physiological salt solution, and anhydrous disodium hydrogen phosphate were purchased from Molar Chemicals Ltd. (Budapest, Hungary). Dodecane and hexane were purchased from Merck KGaA (Darmstadt, Germany). Polar brain lipid extract, porcine stomach mucin (Type III), 1-(3-dimethylaminutesopropyl)-3-ethylcarbodiimide hydrochloride (EDC) were purchased from Sigma Aldrich Co. Ltd. (Budapest, Hungary). Dulbecco's phosphate-buffered saline (DPBS) was acquired from Capricorn Scientific GmbH (Ebsdorfergrund, Germany). As nasal dissolution medium, Simulated Nasal Electrolyte Solution (SNES) was freshly prepared, which consisted of 8.77 g sodium chloride (NaCl), 2.98 g potassium chloride (KCl), 0.59 g and anhydrous calcium chloride ($CaCl_2$) dissolved in 1000 mL of deionized water at pH 5.6. These chemicals were acquired from Sigma-Aldrich Co., Ltd. (Budapest, Hungary).

FAV was provided by Egis Pharmaceuticals Plc. (Budapest, Hungary) with a purity of 99.6% w/w (according to the supplier certificate of analysis). Anhydrous disodium hydrogen phosphate were purchased from Molar Chemicals Kft. (Budapest, Hungary). Acetonitrile 99.8% v/v (HPLC grade) was purchased from PromoChem (Wesel, Germany). Ascorbyl acid-6-palmitate (AP), sorbitan monostearate (Span® 60) and chloroform were purchased from Merck KGaA (Darmstadt, Germany). In all experiments, purified water was filtered using the Millipore Milli-Q® (Merck Ltd., Budapest, Hungary) Gradient Water Purification System.

5. Methods

5.1. Preparation and optimization of lamotrigine-loaded bovine serum albumin nanoparticles (LAM-BSA)

The coacervation method was used to prepare lamotrigine-loaded bovine serum albumin nanoparticles (LAM-BSA) [16]. Firstly, BSA was dissolved in 3 mL of 5 mM NaCl solution under magnetic stirring for 15 min at 40 ˚C. Then, LAM was added to the BSA solution, and the pH was adjusted to 8 with 0.1 N NaOH. Secondly, 15 mL of EtOH was injected dropwise with a flow rate of 1 mL/min until turbidity appeared in the solution. The amount of BSA, the amount of LAM and stirring speed were selected for formulation optimization using Design of Experiments (DoE).

A 3^3 factorial design was used to evaluate the relationship between independent variables (amount of BSA, amount of LAM and stirring speed) and their responses on average hydrodynamic diameter (Y1: Z-average) and encapsulation efficiency (Y2: EE%), as shown in Table 2. The TIBCO Statistica® 13.4 software (Statsoft Hungary, Budapest, Hungary) was used for DoE, quadratic response surface analysis of 2D and 3D plots, and to construct a second-order polynomial model. The relationship of the variables on the response can be analysed by the following second-order equation (1):

$$Y = \beta_0 + \beta_1 X_1 + \beta_2 X_2 + \beta_3 X_3 + \beta_{11} X_1^2 + \beta_{22} X_2^2 + \beta_{33} X_3^2 + \beta_{12} X_1 X_2 + \beta_{13} X_1 X_3 + \beta_{23} X_2 X_3 \qquad (1)$$

Where Y is the response variable; β_0 is a constant; β_1, β_2, and β_3 are linear coefficients; β_{12}, β_{13}, and β_{23} are interaction coefficients between the three factors; and β_{11}, β_{22}, and β_{33} are quadratic coefficients.

Table 2. Independent variables of the 3^3 factorial design

Independent variables	Levels		
	Low (-1)	Medium (0)	High (+1)
X1: Amount of BSA (mg)	10	20	30
X2: Amount of LAM (mg)	10	20	30
X3: Stirring speed (rpm)	500	750	1000

After selecting the optimal formulation, 1 mg of 1-ethyl-3-(3-dimethylaminutesopropyl) carbodiimide hydrochloride (EDC) was added during the preparation process as a cross-linking agent for the stabilization of the nanoparticles after adding EtOH. The cross-linking reaction was conducted for 2 h incubation time at 40˚C using a magnetic stirrer. Then, EtOH was evaporated at 40 ˚C for 30 min under pressure using vacuum drying chambers (Binder GmbH, Tuttlingen,

Germany), and the pellets were redispersed in purified water using an ultrasonication bath. The resulting suspension was purified using a Hermle Z323 laboratory centrifuge (Hermle AG, Gossheim, Germany) at 14000 rpm for 15 min at 4 ± 1˚C. Finally, the pellets were redispersed in purified water to the original volume by using an ultrasonication bath.

5.2. Preparation of favipiravir-loaded aspasomes (FAV-ASP)

Nonionic surfactant-based favipiravir-loaded aspasomes (FAV-ASP) were prepared using a film hydration method [78,79]. Firstly, the lipid solution was prepared by dissolving AP, Span® 60 and CH in 10 mL of chloroform. Secondly, a fixed amount of FAV (30 mg) was dissolved in 5 mL of MeOH (Table 3). Then, FAV solution was mixed with the lipid solution in a round bottom flask, and the organic solvent was evaporated at 60 ℃ and 633 mbar pressure using a Büchi R-210 rotary vacuum evaporator (Flawil, Switzerland), and the rotation was set at 100 rpm for 1 h, until the appearance of a thin film on the wall of the flask. Finally, the thin lipid film was hydrated with 15 mL of pH 7.4 phosphate-buffered saline (PBS) for 1 h.

Table 3. The composition of FAV-ASP formulations

Formulation	Nonionic Surfactant-Based FAV-ASP			
	FAV (mg)	AP (mg)	Span ® 60 (mg)	CH (mg)
FAV-ASP1	30	25	25	50
FAV-ASP2	30	25	50	50
FAV-ASP3	30	50	25	50
FAV-ASP4	30	50	50	50

5.3. Combined methods for LAM-BSA and FAV-ASP formulations

5.3.1. Freeze-drying

Freeze-drying was conducted with a Scanvac, CoolSafe 100-9 Pro type apparatus (LaboGeneApS, Lynge, Denmark). 1.5 mL of all formulations was lyophilized in the presence of 5% w/v mannitol as a cryoprotectant. Freeze-drying was carried out at – 40 ˚C for 16 h under a pressure of 0.012 mbar with an additional 4 h of secondary drying at 25 ˚C. The process was controlled by the Scanlaf CTS16a02 software. The samples were then stored in the refrigerator until further investigation.

5.3.2. Vesicle size analysis, polydispersity index and zeta potential determination

The average hydrodynamic diameter (Z-average), polydispersity index (PDI), and zeta potential (ZP) values of the prepared formulations were evaluated by measuring the dynamic light scattering

using a Zetasizer apparatus (Malvern Instrument Ltd., Worcestershire, UK). The Measurement was carried out using a disposable folded capillary cell at room temperature, and a scattering angle of 173° using He-Ne laser of 633 nm. The formulations were redispersed in distilled water, and then the simples were diluted in distilled water (1:10 v/v) using an ultrasonication bath for 4 min. The measurements were performed in triplicate. The results were presented as means ± SD.

5.3.3. Drug content

Drug content of both LAM-BSA and FAV-ASP formulation was determined as follows: the formulations were redispersed in distilled water, and then 1 mL of the formulations was diluted with 4 mL of methanol using ultrasonication bath for 10 min. After that, the suspensions were filtered using 0.45 µm syringe filters, and LAM concentration was determined using an Agilent 1260 HPLC (Agilent Technologies, San Diego, CA, USA) equipped with a Kinetex® C18 column (5 µm, 150 mm * 4.6 mm, 100 A°). The mobile phase consisted of Methanol: Phosphate buffer (pH 3.5, 10 mM) in a 30:70 (v/v) ratio. The injection volume was 10 µL, with a flow rate of 1 mL/min at 30˚C. Chromatograms were detected at 275 nm [16]. The regression coefficient of the calibration was 0.9997, while the limit of quantification (LOQ) and the limit of detection (LOD) of LAM were 0.016 and 0.049 ppm, respectively. Data were evaluated using ChemStation B.04.03. Software (Agilent Technologies, Santa Clara, USA).

On the other hand, FAV concentration was determined using the same instrument equipped with a Zorbax® SB-CN C18 column (5 µm, 250 mm × 4.6 mm, 100 Å). The mobile phase was acetonitrile–disodium hydrogen phosphate anhydrous buffer (pH 3.1, 20 mM) in a 10:90 (v/v) ratio. The injection volume was 10 µL, with a flow rate of 1 mL/min at 30˚C. Chromatograms were detected at 323 nm [15]. The regression coefficient of the calibration was 0.9996, while LOQ and LOD of FAV were 0.039 and 0.009 ppm, respectively. Data were evaluated using the same software.

5.3.4. Encapsulation efficiency

The encapsulation efficiency (EE%) is defined by the percentage of the drug that is successfully entrapped into the nanoparticles. The EE% of LAM was determined using centrifugation method [33]. The formulations were redispersed in distilled water, and then 1 mL of each sample was centrifuged at 14000 rpm for 15 min at 4 ± 1 ˚C. After that, the clear supernatant solutions were diluted with MeOH, filtered using 0.45 µm syringe filters, and analyzed using the HPLC system. EE% was calculated using the following equation (2):

$$EE\% = \frac{C_{Total} - C_{\text{Supernatant}}}{C_{Total}} \times 100 \quad (2)$$

Where C_{total} is the initial concentration of LAM in the formulation, and $C_{supernatant}$ is the concentration of LAM in the supernatant after centrifugation.

The EE% of FAV was determined using the dialysis method [87]. The formulations were redispersed in distilled water, and then 3 mL of each sample was transferred into a dialysis bag (12 kDa MWCO, Sigma-Aldrich, St. Louis, USA) immersed in 100 mL of purified water and stirred for 30 min. After that, FAV concentration was determined using the HPLC system. All measurements were carried out in triplicate, and the results were presented as means ± SD. EE% and drug loading (DL%) were calculated as follows [88]:

$$EE\% = \frac{C_{before\ dialysis} - C_{after\ dialysis}}{C_{before\ dialysis}} \times 100\% \quad (3)$$

$$DL\% = \frac{Mass\ of\ drug\ encapsulated}{Mass\ of\ nanoparticles\ components} \times 100\% \quad (4)$$

5.3.5. In vitro drug release study under nasal conditions

The drug release test under nasal conditions was conducted using the paddle method (Hanson SR8 Plus (Teledyne Hanson Research, Chatsworth, CA, USA)) [40]. LAM-BSA and FAV-ASP freeze-dried samples were redispersed in SNES (pH 5.6, with a theoretical concentration of 2 mg/mL for both LAM and FAV). Pretreated dialysis membranes (Spectra / Por®,Spectrum Laboratories Inc., Rancho Dominguez, CA, USA) with a molecular weight cut-off value (MWCO) of 12-14 kDa were loaded with 1 mL of the reference suspensions and the samples. The bags were sealed at both ends. 100 mL of SNES was used as a dissolution medium. The measurement was carried out at 32˚C at a paddle rotation speed of 50 rpm, while sampling was carried out for 30 min. Quantification of aliquots was performed by HPLC. Three parallel measurements were performed, and data were presented as means ± SD.

The model-dependent approaches (including zero order, first order, Higuchi model, and Korsmeyer–Peppas model) were used to evaluate the release kinetics of the samples. The DDsolver® add-in software (a menu-driven add-in program for Microsoft Excel) was used for the mathematical evaluation of the release kinetics, and the fit of each model by comparing the rate constant (K), correlation coefficient (R^2), Akaike Information Criterion (AIC), and Model Selection Criterion (MSC) [89–92].

For FAV, the release profiles were also compared with model-independent approaches based on calculating the area under the curve (AUC), dissolution efficiency (DE), and mean dissolution time (MDT).

5.3.6. Rapid equilibrium dialysis measurement (RED)

Time-dependent drug release patterns for the reference suspensions of LAM and FAV, and the samples (LAM-BSA and FAV-ASP) under blood circulation conditions were determined using the RED device (Thermo ScientificTM, Waltham, MA, USA). The reference solutions were prepared by suspending 2 mg of each LAM and FAV in 1 mL of DPBS (pH 7.4) and then homogenizing them in an Eppendorf MixMate vortex mixer (Thermo ScientificTM, Waltham, MA, USA) for 30 sec. RED inserts (8K MWCO) were fitted into the reusable Teflon base plate. The donor chambers were then filled with 150 µL of the reference solutions, as well as the freeze-dried samples redispersed in DPBS. 300 µL of DPBS was used as the acceptor phase, and the base plate was covered with a sealing tape and incubated at 37˚C on an orbital shaker (at 350 rpm) for 4 h. Aliquots were withdrawn at different times from acceptor chambers and immediately replaced with fresh DPBS [69]. Both LAM and FAV concentrations were determined by using HPLC. Five parallel measurements were performed, and the data were presented as means ± SD.

5.3.7. In vitro permeability measurements

A blood-brain barrier-specific parallel artificial membrane permeability assay (BBB-PAMPA) was used to evaluate both LAM and FAV permeability (cm/s) of the initial API solution and the samples [69]. 10 mM of each LAM and FAV was prepared in dimethyl sulfoxide (DMSO), which was further diluted with DPBS solution (pH 7.4) to obtain reference solutions with 100 µM concentration. The donor plate (Multiscreen™-IP, with pore size 0.45 µm; Millipore, Merck Ltd., Budapest, Hungary) was preliminarily coated with 5 µL of lipid solution (24 mg porcine brain polar lipid extract dissolved in 840 µL hexane and 360 µL dodecane). Then, the donor plate was inserted into the acceptor plate (Multiscreen Acceptor Plate, Millipore, Merck Ltd., Budapest, Hungary), which contained 300 µL of DPBS solution (pH 7.4). 150 µL of reference solutions, as well as of the redispersed freeze-dried samples with DPBS in case of FAV (with a nominal concentration of 2 mg/mL of FAV), and the redispersed freeze-dried samples with SNES in case of LAM (with a nominal concentration of 2 mg/mL of LAM) were transferred on the lipid membrane of the donor plate. The plates were incubated at 37 °C for 4 h (Heidolph Titramax 1000, Heidolph Instruments, Schwabach, Germany). After that, the PAMPA plates were separated and both LAM and FAV

concentrations in both donor and acceptor chambers were determined using HPLC. The effective permeability of drugs was calculated using the following equation (5):

$$P_e = -\frac{2.303 \cdot V_A}{A(t-\tau_{ss})} \cdot \log\left(1-\frac{C_A(t)}{S}\right) \quad (5)$$

where P_e means the effective permeability coefficient (cm/s), V_A is the volume of the acceptor well (0.3 cm^3), A indicates the surface area of one well (0.24 cm^2), t is the incubation time (s), τ_{SS} is the time to reach the steady state (s), $C_A(t)$ is the concentration of the compound in the acceptor phase at time point t (mol/cm^3), and S is the solubility of LAM or FAV in the donor phase. The flux of the samples was calculated as follows (6):

$$Flux = P_e \cdot S \quad (6)$$

Six parallel measurements were performed, and data were presented as means ± SD.

5.3.8. Ex vivo nasal permeability study on human nasal mucosa

The *ex vivo* transmucosal permeability of the optimized formulations (LAM-BSA and FAV-ASP) and reference suspensions of LAM and FAV (with 2 mg/mL nominal concentration) was studied in a modified Side-Bi-Side® type horizontal diffusion apparatus under artificial nasal conditions [93]. Human nasal mucosa was collected during routine nasal and sinus surgeries (septoplasty, Functional Endoscopic Sinus Surgery (FESS)) under general or local anesthesia. The surgical field was infiltrated with locally administered 1% lidocaine-adrenalin injection, and the mucosa was excised with a raspatorium or Cottle elevator. Excised nasal mucosa was stored in physiological saline until further investigation. All investigations were conducted freshly within 30 min after the removal of the tissue. The experiments have been performed under the approval of the University of Szeged's institutional ethics committee (ETT-TUKEB: IV/3880-1/2021/EKU). Nasal mucosa was cut with a surgical scalpel into uniform segments with a diameter of 6 mm, and inserted between donor and acceptor phases to provide an appropriate surface for permeability study [94]. To the donor phase 8 mL of SNES was added, whereas to the acceptor phase, 9 mL of DPBS solution (pH 7.4) was pipetted. The temperature of both chambers was thermostated at 32 ± 0.5 °C using a heating circulator (ThermoHaake C 10-P5, Sigma–Aldrich Co. Ltd., Budapest, Hungary). For the measurement, both reference suspensions and selected freeze-dried formulations were redispersed in 1 mL SNES and added to the donor compartment. Both compartments were continuously stirred at 300 rpm using magnetic stirrers. Aliquots were withdrawn (100 µL) from the acceptor phase at 5, 10, 15, 30, and 60 min and replaced with fresh DPBS. The concentrations

were determined using HPLC. The steady-state flux (J_{ss}), permeability coefficient (K_p), and enhancement ratio (*ER*) were calculated as follows [95]:

$$J_{ss} = \frac{m_t}{A \times t} \quad (7)$$

$$K_p = \frac{J_{ss}}{C_d} \quad (8)$$

$$ER = \frac{J_{ss}\ formulation}{J_{ss}\ Reference} \quad (9)$$

Where J_{ss} is the steady-state flux (μg/cm^2/h), m_t is the permeated drug quantity through the nasal mucosa, A is the surface of the membrane insert (0.785 cm^2), t is the duration of the investigation, K_p the permeability coefficient (cm/h) and C_d is the drug concentration in the donor phase (μg/cm^3).

5.4. Methods related to characterization of LAM-BSA

5.4.1. In vitro assessment of mucoadhesive property

Mucin 1% (w/v) was prepared in SNES (pH 5.6) and the mixture was stirred continuously overnight at 37 ˚C. Subsequently, the size of the mucin particles was reduced to 200–300 nm using a probe sonicator for 1 min. The suspension was then centrifuged at 4000 rpm for 20 min to remove the aggregates and the supernatant was used for the test [96]. For testing, the optimal formulation (after redispersion in 1.5 mL of purified water) was incubated with 1% (w/v) mucin suspension in the ratio 1:1 (v/v) at 25 ˚C for 1 h. Then, the zeta potential was measured using a Malvern Zetasizer Nano ZS (Malvern nano ZS, Malvern Instruments, Worcestershire, UK) as described previously. All measurements were carried out in triplicate, and the results were presented as means ± SD.

5.4.2. Cytotoxicity assay

Cytotoxicity was determined by the MTT assay on the human colon adenocarcinoma (Caco-2) cell line. Caco-2 cells were kindly donated by Solvo Biotechnology (Szeged, Hungary). The cells were cultivated in Dulbecco's modified essential medium. The medium was supplemented with 10% fetal bovine serum, 1% non-essential amino acids, and 1% antibiotic-antimycotic complex (penicillin, streptomycin, amphotericin B). Cells were incubated at 37˚C in a humidified

atmosphere containing 5% CO2. Cells were seeded in 96-well plates (50.000 cells/well) and after overnight incubation, the formulations were added at six different concentrations (5, 10, 25, 50, 100, and 250 μM for LAM) and incubated for two hours under cell culture conditions. Finally, 20 μL of 5 mg/mL MTT solution was pipetted to each well and incubated for an additional 4 h. Then, the medium was removed, and the precipitated formazan crystals were dissolved in DMSO by shaking at 37 ˚C for 30 minutes. Absorbances were measured at 545 nm using a microplate reader (SPECTROStar Nano, BMG Labtech) [97]. Cell viability was assessed using the statistical software GraphPad Prism 10.12 and was calculated using the following equation (10):

$$Cell\ viability\ \% = \frac{Mean\ OD\ of\ sample}{Mean\ OD\ of\ control\ group} \times 100 \quad (10)$$

Where OD represents the optical density, which is a measure of the absorbance of the samples [98,99].

5.4.3. Permeability study on Caco-2 permeability model

The permeability coefficients across the Human colon adenocarcinoma cells monolayer (Caco-2) were determined to predict the absorption of the tested formulations of LAM. Caco-2 cells were harvested and seeded on filter supports (polycarbonate membrane, 0.4 μm pore size, 1.12 cm^2 in 12-well plates, Corning Costar Co., Lowell, MA, USA) at a density of 300.000 cells/insert. Cells were cultivated in 12-well plates with 1.5 mL medium in the acceptor and 0.5 mL of medium in the donor phase. The inserts were incubated at 37 ºC, 5% CO2 concentration in a humidified atmosphere for 21-29 days. The medium was changed every second day in the donor and acceptor phases.

The tightness of the Caco-2 cell layer was verified by measuring transepithelial electric resistance (TEER), which represents the closure of the cell layer of the epithelial barrier. TEER was measured with a Millipore Millicell ERS-2 voltohmmeter (Merck, USA) combined with STX-2 electrodes, and was calculated to the surface area of the monolayers as $\Omega \times cm^2$. The cells were treated with the formulations when the cell layer reached steady-state TEER values.

During permeability experiments, the inserts were placed on 12-well plates containing 1.5 mL of physiological saline solution in the acceptor compartments (lower/base). In the donor compartments (upper/apical), the culture medium was changed, and 0.5 mL of the tested formulations was added in saline. After incubation, samples were collected from the donor and

acceptor compartments, and the LAM concentrations were measured by HPLC [100]. The apparent permeability coefficients (P_{app}) were determined according to the following equation (11) [101]:

$$P_{app} = \frac{\Delta[C]_A \times V_A}{A \times [C]_D \times \Delta t} \quad (11)$$

Where P_{app} is the apparent permeability (cm/s), $\Delta[C]_A$ is the difference in the concentration in the acceptor compartment after 120 min, $[C]_D$ is the initial concentration in the donor compartment, V_A is the volume of the acceptor compartment (1.5 mL) and A is the surface area available for permeability (1.1 cm^2).

5.5. Methods related to characterization of FAV-ASP

5.5.1. Droplet size distribution measurement

Laser diffraction method was used to evaluate the droplet size distribution of the optimal formulations [4]. The evaluation was performed using a Malvern Spraytec® system (Malvern Instruments Ltd., Malvern, UK), equipped with a 300 mm lens capable of analysing droplet sizes in a range of 0.1–900 μm (Dv50: 0.5–600 μm). The tip of the nasal spray device was aligned and positioned at 45° from the horizontal plane. Measurements were conducted at room temperature. The optimal formulation was redispersed in distilled water and placed in a nasal spray container. Each nasal spray was manually actuated three times and discharged into waste, allowing the device to function optimally. The data were analyzed using the Spraytec® software v4.00 (Malvern Panalytical Ltd., Malvern, UK), with volume diameter and described as 10% (Dv10), 50% (Dv50), and 90% (Dv90) of the cumulative volume distribution. The results were presented as means ± SD.

5.5.2. Storage stability

The optimal formulation was stored at 4 °C and the storage stability study was conducted for 4 weeks, and analyzed in terms of Z-average, PDI, ZP to evaluate the physical stability and in terms of drug content to evaluate the chemical stability every week (as described previously).

5.5.3. In vivo study

5.5.3.1. Animals and samples collection

The animals were kept at room temperature (approximately 23 °C) and light was adjusted to alternate darkness and light for 12 hours. The rats were fed with normal rodent chow and tap water ad libitum. All animals received humane care, in compliance with the "Principles of Laboratory Animal Care" according to the National Society for Medical Research and the Guide for the Care and Use of Laboratory Animals, formulated by the National Academy of Sciences, and published by the National Institute of Health (NIH Publication No. 86-23, revised 1985). Healthy male Sprague-Dawley rats (339 ± 39 g, mean ± SD) were anaesthetized with an *i.p.* injection of ketamine (50 mg/kg) and xylazine (10 mg/kg). The femoral vein was cannulated for plasma collection [102]. A total of 50 µL FAV (2 µg/µL) or the corresponding formulation of FAV was administered nasally. Animals were divided into two groups (FAV and optimal FAV-ASP), and 0.5 mL of blood samples were taken at 0, 5, 10, 15, 30 and 60 min post-FAV administration, then cerebrospinal fluid samples were collected at the end of the experiments. After 45 min, the clot was removed by centrifuging at 1000 x g for 10 min. The resulting supernatant (non-hemolytic serum) was extracted with 2 volumes of acetonitrile. Accordingly, acetonitrile is suitable for precipitating and removing high-abundance proteins from the serum and eliminating the intra-molecular protein interactions. The precipitate was removed by centrifuging at 1000 × g for 10 min.

5.5.3.2. Sample preparation

Real or spiked (standard) plasma or cerebrospinal fluid samples were precipitated with acetonitrile (1:2) and centrifuged at 1000 x g for 10 min. The supernatants were collected, and the samples were dried under a gentle stream of N_2 at 60 ℃ using a Turbovap LV concentrator. The samples were re-dissolved in 50 µL pyridine, and then 50 µL *N*,*O*-bis(trimethylsilyl)tri- fluoroacetamide (BSTFA) with 1% of trimethylchlorosilane (TMCS) was added into the tubes. The solutions were transferred into 1.5 mL vials sealed, and derivatization was carried out at 80 ℃ for 30 min at 500 rpm using an Eppendorf Thermomixer C device [103]. Finally, 1 µL of the reaction mixture was injected into GC-MS equipment.

5.5.3.3. Gas chromatograph-mass spectrometric (GC-MS) analysis

Derivatized FAV was measured by GC-MS using a Shimadzu GCMS-QP2010 (Shimadzu, Kyoto, Japan) equipment. The GC was equipped with an SLB-5 MS capillary column (Supelco, Bellefonte, PA, USA) (30 m × 0.25 mm i.d.; 0.25 µm film thickness). Operating conditions were as follows: carrier gas: He, flow rate 32 cm/s; column temperature program: 1 min at 60 °C, 60-250 °C at 40 °C/min and finally 7 min at 250 °C. The temperature of the injection port and the interface were 250 °C and 270 °C, respectively. 1 µL of the samples was injected into the GC-MS using an AOC-20i autosampler; the split ratio was 1:10. The MS was equipped with an electron ionization (EI) ion source, and the operating conditions were as follows: ionization energy 70 eV, ion source temperature 200 °C, solvent cut time 4 min. The measurements were carried out in selected ion monitoring (SIM) mode. The registered ions were 301 m/z, 286 m/z and 270 m/z, which were selected based on the EI spectrum measured in SCAN mode.

5.5.3.4. Evaluation of pharmacokinetic (PK) parameters

The PK parameters of initial FAV and FAV-ASP1 were determined in the plasma and the CSF following a single intranasal dose to evaluate the brain targeting. PK Solver 2.0 software was used to determine pharmacokinetic parameters by non-compartmental analysis [104]. The maximum concentrations (C_{max}) and times taken to reach these concentrations (T_{max}) were determined from the mean concentration-time profiles. The elimination rate constant (k_e) was determined by plotting log-linear concentration versus time. The elimination half-life ($t_{1/2}$) was calculated using equation (12) [105]:

$$t_{1/2} = 0.693/k_e \tag{12}$$

The area under the plasma concentration versus time curve ($AUC_{0\text{-}t}$) was calculated using the linear trapezoidal method from time 0 to time t (the last time point to withdraw blood samples), then the AUC from 0 to infinity, $AUC_{0-\infty}$ (µg hour/mL) was calculated using the following equation [105,106]:

$$AUC_{0-\infty} = AUC_{0-t} + C_t/k_e \tag{13}$$

where C_t (µg/mL) is the last measured concentration at time t.

The clearance (C_L), the apparent volume of distribution (V_d), the mean residence time (MRT), and the relative bioavailability (F%) were calculated using the following equations [69,107–110]:

$$C_L = dose/AUC_{0-\infty} \quad (14)$$

$$V_d = \frac{C_L}{k_e} \quad (15)$$

$$MRT = \frac{\int C\,.tdt}{\int Cdt} = \frac{AUMC}{AUC} \quad (16)$$

$$F\ (\%) = \frac{(AUC_{0-t})_{formulation}}{(AUC_{0-t})_{reference}} \times 100 \quad (17)$$

where AUMC is the first moment of the concentration-time integral.

5.5.3.5. Evaluation of in vitro-in vivo correlations (IVIVC)

A point-to-point IVIVC for initial FAV and FAV-ASP1was mathematically examined based on the in vitro and the *in vivo* pharmacokinetics data (based on FDA guidance [111–113]). The relationship between *in vitro* values of $AUC_{0\text{-}t}$ (µg×min/mL) and *in vivo* values of AUC0-t (µg×min/mL) was evaluated using linear regression. R^2 values have been calculated for each graph.

5.6. Statistical analysis

All results are expressed as mean ± SD. GraphPad Prism version 10.12 software (GraphPad Software, San Diego, CA) was used for the statistical analysis. A one-way analysis of variance (ANOVA) and Tukey's post-hoc test were performed to compare the groups. A significant level was set at a p value < 0.5. Where (ns) means non-significant, *p-value < 0.05, **p-value < 0.01, and ***p-value < 0.001, ****p-value <0.0001.

6. Results and Discussion

6.1. Results of LAM-BSA characterization

6.1.1. Preparation and optimization of LAM-BSA

LAM-BSA nanoparticles were prepared using the coacervation method, which is one of the most commonly used processes to prepare albumin nanoparticles. The use of EtOH, as a desolvating agent, decreases the solubility of BSA, causing phase separation and conformation changes in albumin structure, including the shrinkage of the hydrated BSA chains [114]. These changes result in coacervation or precipitation of the albumin in the form of nanoparticles [115]. In this study, we used 15 mL of EtOH (5 times higher volume than the BSA solution). It was suitable for the BSA to become supersaturated, precipitate, and result in the formation of small and uniform particles with a narrow size distribution [116].

In this study, we studied the effect of BSA amount (X1), LAM amount (X2) and the stirring speed (X3) on the Z-average (Y1) and EE% (Y2) of the prepared nanoparticles at 3 levels (Table 4).

Table 4. Dependent and independent factors of the 3^3 factorial design. Results are presented as mean ± SD

Formulation Code	Independent factors			Responses	
	BSA (mg)	LAM (mg)	Stirring speed (rpm)	Z-average (nm)	EE (%)
LAM-NP-1	10	10	500	184.90 ± 0.82	62.76 ± 4.53
LAM-NP-2	10	20	1000	212.50 ± 1.73	83.01 ± 4.29
LAM-NP-3	10	30	750	218.83 ± 3.00	89.290 ± 2.88
LAM-NP-4	20	10	1000	205.77 ± 2.51	66.56 ± 3.94
LAM-NP-5	20	20	750	223.23 ± 2.24	83.27 ± 5.60
LAM-NP-6	20	30	500	182.73 ± 1.58	89.59 ± 3.45
LAM-NP-7	30	10	750	195.87 ± 0.85	64.84 ± 2.09
LAM-NP-8	30	20	500	168.90 ± 4.04	86.53 ± 3.11
LAM-NP-9	30	30	1000	173.80 ± 1.25	91.78 ± 2.46

As shown in Table 4, the prepared formulations had an accepted Z-average value ranging from 168.90 ± 4.04 to 223.23 ± 2.24 nm. Nanoparticles with Z-average values < 200 nm can bypass the BBB and escape from the reticuloendothelial system [117]. Furthermore, the EE% was higher than 50%, which means that BSA nanoparticles successfully encapsulated LAM.

A. The impact of independent factors on Z-average (Y1)

A quadratic equation describing the individual main effects of X_1, X_2, and X_3 on Y_1 was generated by the reduced linear mathematical model, as presented in equation (18):

$$Y1 = 196.281 - 12.944X_1 - 1.861X_2 + 9.255X_3 + 3.994X_1^2 + 3.947X_2^2 + 12.272X_3^2 - 3.455X_1X_2 \quad (18)$$

The regression coefficient (R^2) of the surface plot was 0.999, the adjusted R^2 was 0.997 and the MS Residual was 0.022, indicating a proper correlation. The R^2 values demonstrate how well the predicted model fits the experimental data, and its value should be closer to 1. The R^2 adjusted is another modified form of R^2 that demonstrates the number of terms present in the model [118]. Analysis of variance (ANOVA) was applied as statistics, with a 95% confidence interval level, where the variable was considered significant if the p-value < 0.05. The results showed that the p-values of the model for Y_1 were less than 0.05, which justifies the fact that the quadratic model is significant. The model factors such as X_1, X_3, X_1^2 were significant (p-value < 0.05). The equation in terms of actual factors can be used to make predictions about the response for given levels of each factor. According to these results, the increase in the amount of BSA led to a decrease in the Z-average (significant effect). Furthermore, the effect of LAM amount was insignificant and negligible on Z-average. The results showed that the Z-average increased with increasing stirring speed, but after a certain stirring speed, the Z-average was unaffected by the rate of stirring (Figure 2). Then, it started to decrease with increasing stirring speed. A similar result was obtained by Rahimnejad et al. [81].

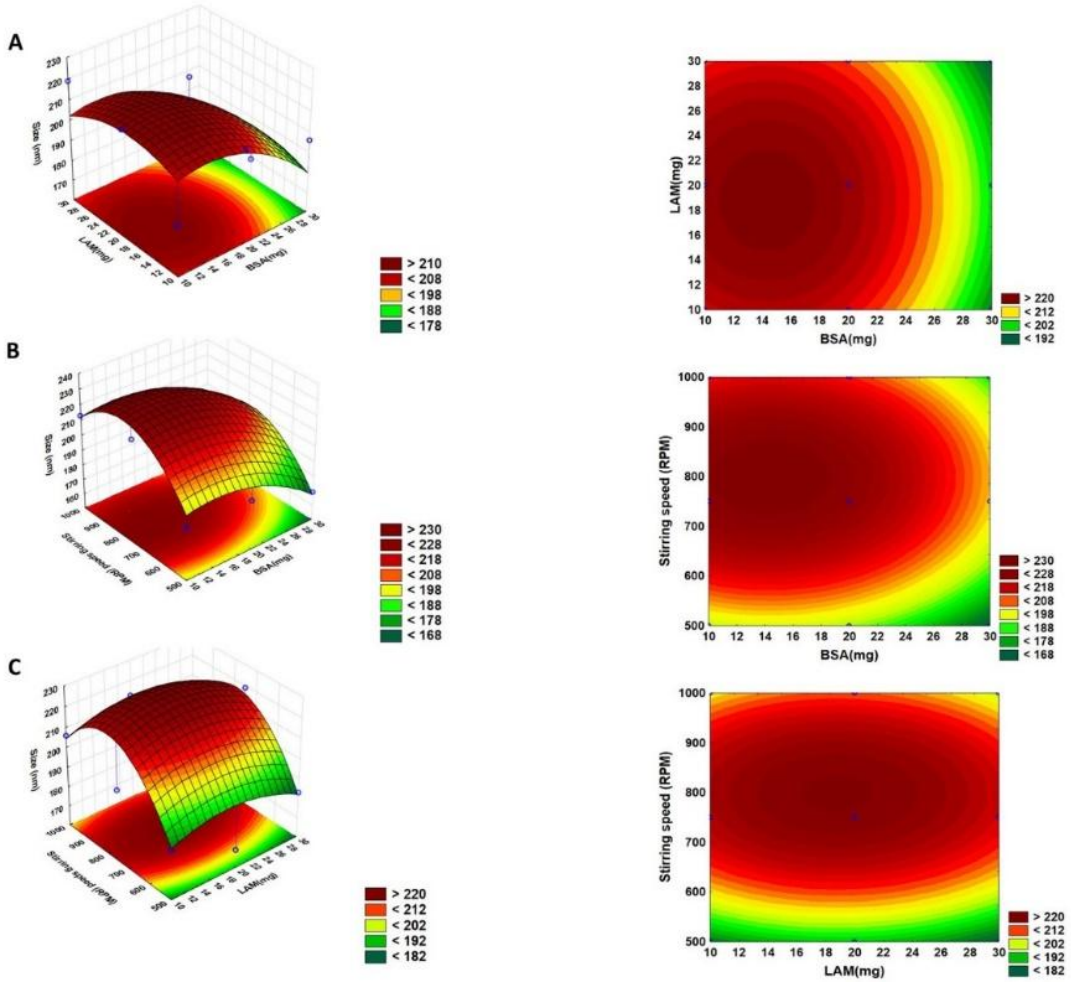

Figure 2. Contour plots (2D) and response surface plots (3D) of selected independent factors on Z-average; (A): BSA amount (X_1) and LAM amount (X_2), (B): BSA amount (X_1) and stirring speed (X_3), (C): LAM amount (X_2) and stirring speed (X_3).

B. The effect of independent factors on EE%

A quadratic equation describing the individual main effects of X_1, X_2, and X_3 on Y_2 was generated by the reduced linear mathematical model, as presented in equation (19):

$$Y2 = 79.737 + 1.348X_1 + 12.747X_2 + 3.4X_2^2 \quad (19)$$

The regression coefficient (R^2) of the surface plot was 0.992, the adjusted R^2 was 0.988, and the MS Residual was 1.545, which indicates a proper correlation. The results showed that the p-values of the model for Y_2 are less than 0.05, which justifies the fact that the quadratic model is significant. The model factors such as X_1, X_2, X_2^2 were significant (p-value < 0.05, p-value < 0.001, p-value < 0.001, respectively), and had positive effects. The results showed that the EE% increased with increasing amount of BSA (Figure 3). Similar result obtained by Sailaja et. al. [119]. This can be

related to the availability of higher amounts of polymer for entrapment. Moreover, the EE% increased with increase of the LAM amount. Maghsoudi et al. found that EE% increases with drug concentration [120].

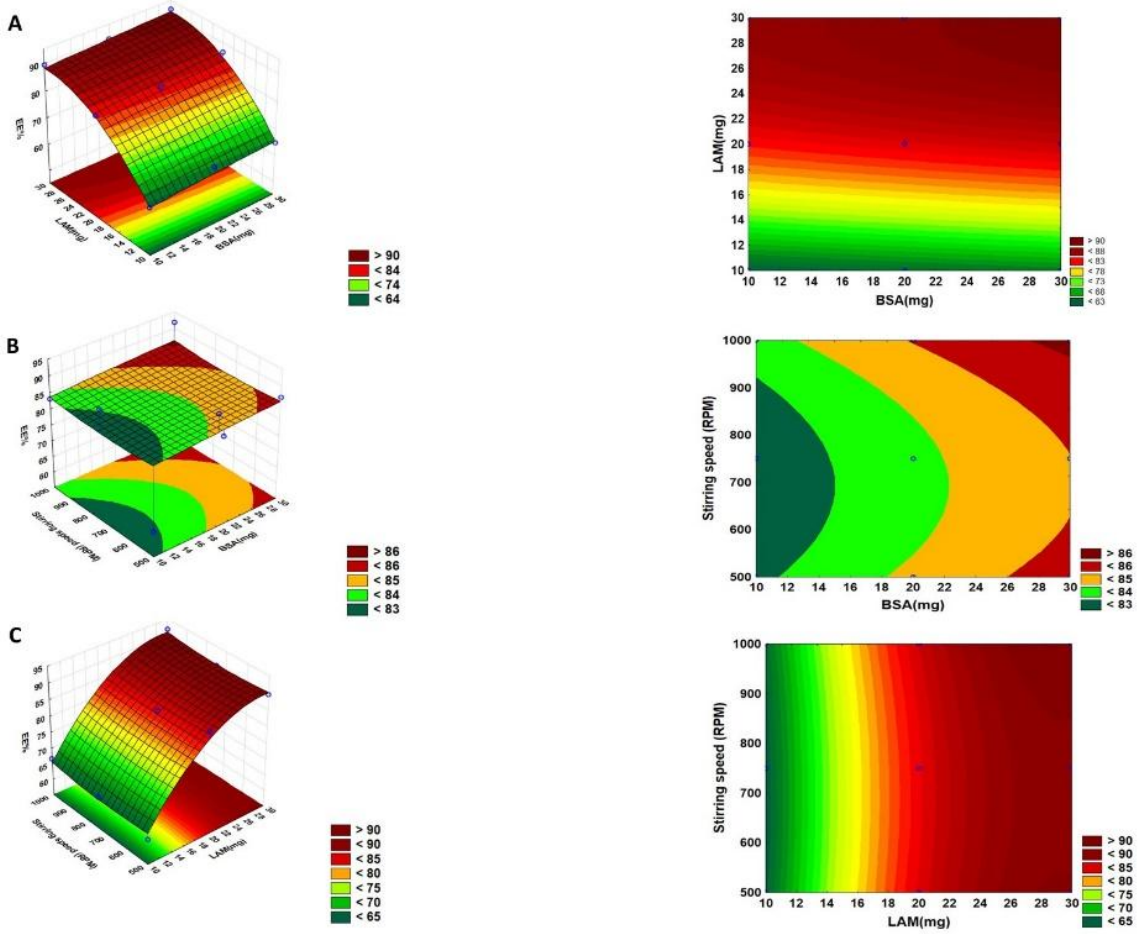

Figure 3. Contour plots (2D) and response surface plots (3D) of selected independent factors on EE%; (A): BSA amount (X_1) and LAM amount (X_2), (B): BSA amount (X_1) and stirring speed (X_3), (C): LAM amount (X_2) and stirring speed (X_3).

Based on these results, the selected LAM-NP was prepared using: BSA (30 mg), LAM (30 mg), and the stirring speed (1000 rpm). The particle size was 173.80 ± 1.25 nm with a narrow particle size distribution (PDI = 0.21 ± 0.01), a negative ZP value (-29.80 ± 0.07 mV) and a high EE% value (91.78 ± 2.46 %). Z-average, PDI and ZP are considered important parameters which could influence drug release, cellular uptake, biodistribution and stability [121]. PDI value showed a narrow particle size distribution (PDI < 0.3), which means the potential for the formation of uniform nanoparticles with lower aggregation and hence improved the stability. The negative ZP value (> -30 mV) indicating higher physical stability due to the electrostatic repulsive forces that

prevent albumin nanoparticles from aggregating, and a long-circulating system which increasing permeability through the BBB and into the brain [122]. This formulation was used for the cross-linking reaction with EDC (1 mg) to prepare the optimal LAM-BSA formulation.

Cross-linking is essential for nanoparticle preparation, affecting the stability, bio-decomposability and drug release from the nanocarrier due to the impact on Z-average, PDI, ZP, and EE%. EDC is a zero-space cross-linker. It forms peptide bands between carboxyl and amide groups of amino acids in stabilized nanoparticles to form active O-urea, creating an amide link with amino groups and releasing water-soluble, easily removable isourea [123]. The primary amines of free LAM could be sites of this nucleophilic reaction.

The freeze-dried LAM-BSA formulation (with Z-average of 163.77 ± 1.96 nm, PDI of 0.16 ± 0.01, ZP value of -33.97 ± 0.59 mV, and a high EE% value of 97.31 ± 0.17 %) was used for further investigations.

6.1.2. In vitro drug release at nasal conditions

Drug release is an important parameter for evaluating the efficiency of the drug carrier in comparison to the initial drug and predicting the drug performance after IN administration. LAM is a BCS Class II drug, and its dissolution is the rate-limiting step for its absorption. Since LAM is a weak base, it may not have dissociated efficiently above its pKa value (5.7), which limits drug solubilization at pH 5.6, which could be responsible for the lower degree of drug release from BSA nanoparticles. The results of cumulative in vitro release of the optimal LAM-BSA formulation in comparison to initial LAM is presented in Figure 4. The results demonstrated that there was no significant difference in the release profile of LAM-BSA formulation and initial LAM up to 30 min.

The release of LAM from BSA nanoparticles followed two mechanisms: albumin degradation and diffusion through the pores [124]. DDsolver® was used to evaluate the release kinetics for the optimal formulation at pH 5.6. The model with the highest R^2 value, with low AIC and the high MSC values is the best kinetics model (Table 5). The results showed that the release profile fitted the Korsmeyer-Peppas kinetic model. The release exponent "n" value was 1.245 (n > 0.89), which reflects the super case II transport mechanism [125]; therefore, the release is ruled by the relaxation dynamics of the polymeric macromolecular chains.

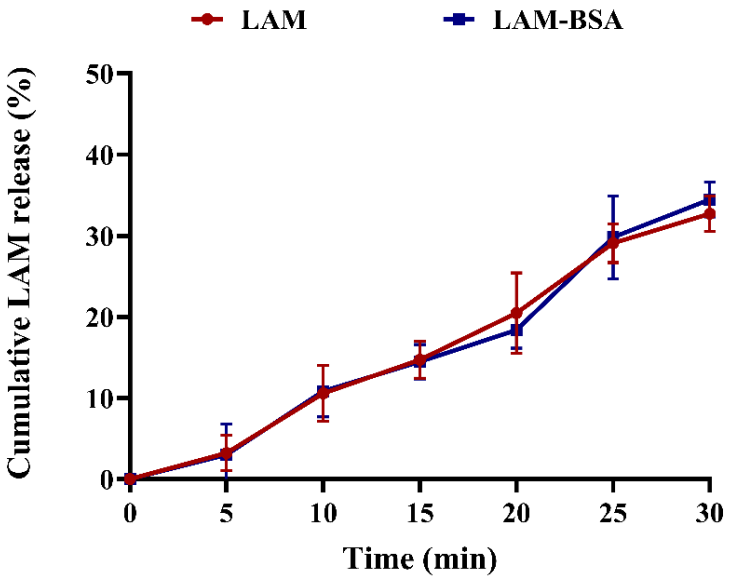

Figure 4. Cumulative *in vitro* release profile of LAM-BSA in comparison with the initial LAM. Results are expressed as means ± SD (n = 3).

Table 5. Comparison of release profiles (at SNES pH 5.6) using model dependent approaches

Model Parameters	Zero-order	First-order	Higuchi	Korsmeyer-Peppas
k	1.093	0.013	4.942	0.505
R^2	0.968	0.949	0.794	0.983
AIC	25.998	29.376	39.213	23.367
MSC	2.891	2.408	1.003	3.266

6.1.3. Rapid equilibrium dialysis measurement (RED)

RED is an accurate method to examine drug-protein binding directly in the biological fluid at the site of action. It uses a size-defined dialysis membrane to quantify active drug molecules that are not bound to plasma proteins in an equilibrium state [126].

The cumulative *in vitro* release of the optimal LAM-BSA formulation in comparison to initial LAM was investigated at blood circulation conditions (pH 7.4). The results demonstrated that the release of LAM from LAM-BSA formulation increased compared to the initial LAM (p-value < 0.05), as shown in Figure 5. This increase in release rate might be attributable to the pH-dependent solubility of LAM, as well as the high encapsulation efficiency, the smaller particle size, which gives a higher surface area that increases drug release.

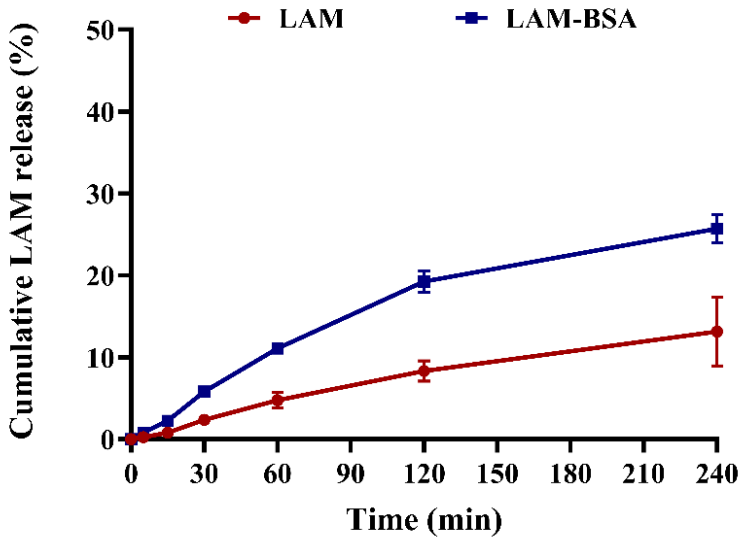

Figure 5. Rapid equilibrium dialysis (RED) of the selected formulations in comparison with the initial LAM. Results are expressed as means ± SD (n = 5).

6.1.4. In vitro permeability measurements

BBB-PAMPA is a useful tool to evaluate the drug's passive transportation through the nasal epithelium and BBB but has difficulty predicting paracellular and active transport [4]. The results demonstrated that BSA-LAM formulation had significantly higher flux values than the initial LAM (p-value < 0.0001), as shown in Figure 6. We could explain this result by the enhancement in LAM solubility due to using BSA nanoparticles as a drug carrier.

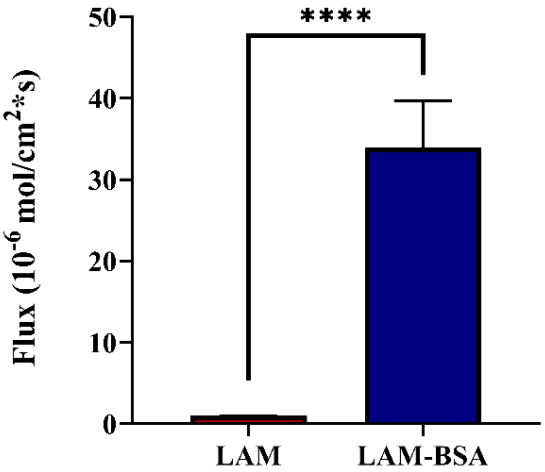

Figure 6. Fluxes of the PAMPA permeability study of LAM-BSA formulation in comparison with the initial LAM. Results are expressed as means ± SD (n = 6). ****p-value <0.0001.

6.1.5. In vitro assessment of mucoadhesive property

Nasal mucociliary clearance poses a major challenge for nasal drug delivery, as it can reduce the residence time of formulations to approximately 15 to 30 min [127]. Therefore, it is crucial to evaluate the mucoadhesive properties of LAM-BSA formulation. In this study, we used electronic theory to evaluate the mucoadhesive properties by measuring ZP through the interaction of negatively charged nanoparticles after incubation with mucin 1% (1:1 v/v) for 1 h. Mucin 1% showed a negative ZP value of -4.75 ± 0.36 mV. LAM-BSA showed a high decrease in ZP values (from -33.97 ± 0.59 to -11.36 ± 0.11 mV) after 1 h of incubation with mucin 1%. The formation of a mucin layer covering nanoparticles can explain the enhanced interaction observed between LAM-BSA and mucin. This strong interaction indicates improved mucoadhesive properties, which are crucial for nasal drug delivery. The intimate contact between nanoparticles and the nasal mucosa, facilitated by these interactions with mucin, significantly contributes to prolonging the residence time of the drug formulation in the nasal cavity. Consequently, utilizing BSA nanoparticles increases the duration the drug remains at the application site, improving its absorption and enhancing its bioavailability.

6.1.6. Cytotoxicity assay

The percentage of cell viability was determined after incubation the cells with LAM at a concentration of 5-250 μM for 2 h. The results of initial LAM demonstrated a significant decrease in cell viability from 93.80 ± 1.29 % to 70.71 ± 2.05 %, while LAM-BSA demonstrated a decrease in cell viability from 97.31 ± 0.78 % to 82.43 ± 1.48 % (Figure 7). This result indicated that LAM-BSA formulation is non-toxic (cell viability > 70 % [128]), and the use of BSA nanoparticles could be a suitable and compatible drug carrier for LAM to decrease its toxicity. A similar result was obtained by Shankar Raman et al. [129].

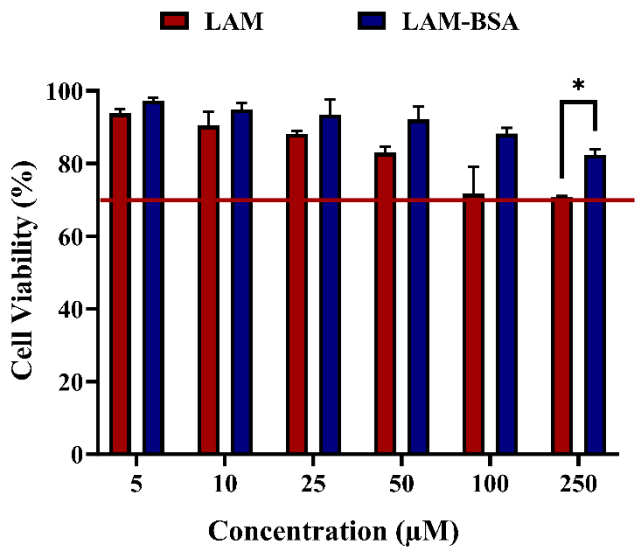

Figure 7. Cell viability % of LAM-BSA formulation in comparison to the initial LAM. Results are expressed as means ± SD (n = 3). *p-value < 0.05.

6.1.7. Permeability Study on the Caco-2 cell monolayer

The Caco-2 cell line, derived from human colon adenocarcinoma, is widely used as an *in vitro* model to study and predict transcellular absorption mechanisms such as passive diffusion, active transport, efflux, and paracellular transport. Due to their ability to form a tight paracellular barrier, Caco-2 cells serve as valuable models for predicting nasal drug absorption, as the tight junctions and transport properties of Caco-2 cells mimic important aspects of the nasal epithelial barrier. The permeability of LAM from LAM-BSA formulation compared to the initial LAM at a concentration of 100 µM is presented in Figure 8. The results showed that LAM-BSA had a higher P_{app} value compared to pure LAM (non-significant effect). This indicates that BSA nanoparticles may improve LAM nasal absorption by promoting transport into cells. Furthermore, Caco-2 cells also express numerous metabolic enzymes such as cytochrome P450 isoenzymes (CYP450) and some phase II enzymes (e.g., glutathione-S-transferases, sulfotransferase and glucuronidase) which may degrade BSA-NP and release LAM [16].

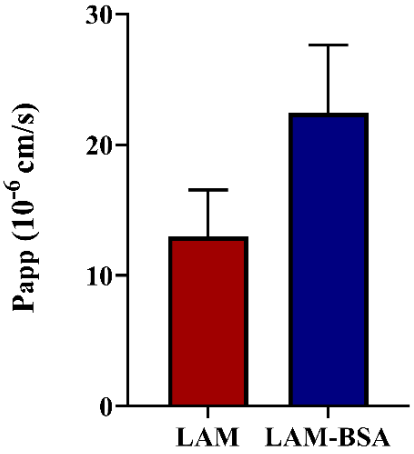

Figure 8. P_{app} value of LAM-BSA formulation compared to the initial LAM at a concentration of 100 µM. Results are expressed as means ± SD (n = 3).

6.1.8. Ex Vivo Nasal Permeability Study on Human Nasal Mucosa

Human nasal mucosa has been used to predict the absorption of the LAM-BSA formulation through the nasal cavity, and to predict the penetration across the BBB. The test exposure time was 60 min, which is considered appropriate for nasal excipients/drugs due to rapid nasal mucociliary clearance by nasal mucociliary activity. The result demonstrated that the optimal formulation (LAM-BSA) exhibited a significantly higher cumulative permeated amount of LAM compared to the initial LAM (p-value < 0.05), (260.61 ± 0.66 and 841.71 ± 2.09 µg/cm^2 for LAM and LAM-BSA, respectively), as shown in Figure 9.

We could explain this result by considering that LAM-BSA formulation had a small particle size of 163.77 ± 1.96 nm, which is within the typical range of intrinsic mucus pore sizes (20-200 nm) [130]. As reported in the literature, nanoparticles ranging from 100 to 700 nm can be transported intracellularly through the nasal epithelium and could reach the brain via the olfactory neural pathway [131].

Furthermore, BSA, as a bioadhesive polymer, increases the contact time of LAM-BSA with the nasal mucosa, thereby enhancing absorption through the nasal epithelium.

The biopharmaceutical parameters, including steady-state flux (Jss), permeability coefficient (Kp) and enhancement ratio were summarized in Table 6. The results indicated a significant enhancement in the biopharmaceutical parameters of LAM-BSA compared to initial LAM.

Table 6. The biopharmaceutical parameters of LAM-BSA compared to the initial LAM. Results

are expressed as means ± SD (n = 3).

Sample	Flux (µg/cm²/h)	K_p (cm/h)	ER
LAM	4.34 ± 0.01	0.006	-
LAM-BSA	14.07 ± 0.11[a]	0.013 [a]	3.24 ± 0.03

Notes: [a] p-value < 0.0001.

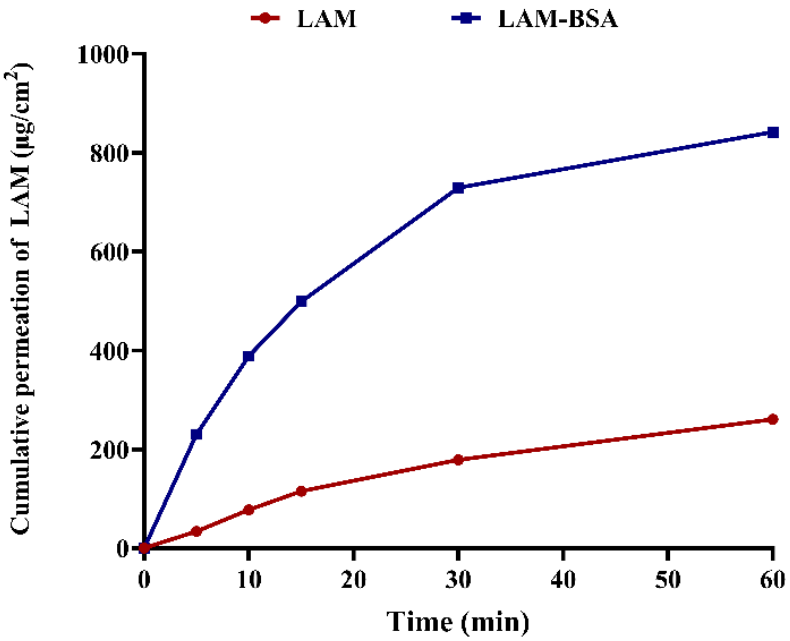

Figure 9. Ex vivo permeability study of the optimal formulations in comparison with initial LAM on human nasal mucosa. Results are expressed as means ± SD (n = 3).

6.2. Results of FAV-ASP characterization

6.2.1. Preparation and optimization of FAV-ASP

FAV-ASP formulations were prepared by combining different amounts of AP and nonionic surfactants (Span® 60) with fixed amount of CH. AP was used for the fabrication of ASP due to its hydrophilic-lipophilic balance (HLB) value (8.4), which is suitable for formation the vesicles [132]. However, it is important to combine AP with CH and Span® 60 to improve the stability of ASP vesicles [133,134]. CH provides rigidity to the bilayer membrane of the vesicles; therefore, enhance their physical stability. Moreover, Span® 60 was used as a stabilizer due to its long chain length (C18), which leads to a higher encapsulation efficiency. The temperature of the rotary evaporator was 60 °C, above the gel-to-liquid phase transition temperature of Span® 60 (53−55 °C) [79,135].

For the optimization, we first selected formulations based on the acceptable parameters of the drug carrier for the nose-to-brain delivery system, which include: a Z-average of 150–300 nm, PDI < 0.5, ZP > |±30| mV, EE% > 50%, and DL% > 10% [5,136,137], to be evaluated using BBB-PAMPA.

As presented in Table 7, only FAV-ASP4 had a Z-average > 300 nm; therefore, we excluded it from the evaluation. On the other hand, FAV-ASP2 showed EE% and DL% values out of the acceptable range; thus, we also excluded it from further investigation.

Table 7. Z-average, PDI, ZP and EE% values of the prepared formulations. Results are expressed as means ± SD (n = 3).

Formulation	Z-average (nm)	PDI	ZP (mV)	EE (%)	DL%
FAV-ASP1	292.06 ± 2.10	0.36 ± 0.03	-74.73 ± 3.28	55.33 ± 0.41	12.79 ± 0.22
FAV-ASP2	292.76 ± 3.80	0.31 ± 0.05	-73.16 ± 4.65	48.35 ± 0.38	9.374± 0.07
FAV-ASP3	284.60 ± 6.70	0.29 ± 0.06	-65.66 ± 2.70	53.48 ± 0.26	10.36 ± 0.41
FAV-ASP4	341.20 ± 8.88	0.40 ± 0.04	-72.82 ± 1.20	-	-

The results demonstrated that with the increase in AP amount, the Z-average significantly decreased (p-value < 0.0001). While with the increase in Span® 60 amount, the Z-average significantly increased (p-value < 0.0001), which could be due to an increase in CH amount to fill the gaps and counteract the effect of Span® 60, leading to higher rigidity to the bilayer membrane of the vesicles. The formulations showed acceptable PDI values < 0.5, which reflects a relatively homogeneous. Moreover, ZP values were > -30 mV, indicating high physical stability of the vesicles due to the electrostatic repulsive forces that prevent particle aggregation [137]. Furthermore, EE% increased significantly by increasing the amount of Span® 60 (p-value < 0.0001), or by increasing the amount of AP (p-value < 0.01), or by increasing both AP and Span® 60 amounts (p-value < 0.0001).

6.2.2. In vitro permeability measurements

As we mentioned previously, BBB-PAMPA is a useful tool to evaluate of the drug passive transportation through the nasal epithelium and BBB. In this study, we used BBB-PAMPA to select the most promising formulations, hence to reduce *in vitro* and *in vivo* tests.

The results demonstrated that the selected formulations (FAV-ASP1 and FAV-ASP3) had a significantly higher permeability than initial FAV (**p-value < 0.01, and ***p-value < 0.001, respectively). We could explain this result by the effect of Span® 60, which improves the solubility

of FAV and increases its permeability through the porcine brain polar lipid extract. This effect could be observed in the flux values (Figure 10B).

Based on Figure 10A and B, we selected FAV-ASP1 as the optimal formulation, which had the smallest particle size (292.06 ± 2.10 nm), an acceptable PDI (0.36 ± 0.03), a negative ZP value (-74.73 ± 3.28 mV), the highest EE% and DL% values (55.33 ± 0.41% and 12.79 ± 0.22%, respectively), and the highest permeability and flux values of 23.78 ± 2.84 (10^{-6} *cm/s) and 51.47 (10^{-6} *mol/cm^2*s), respectively.

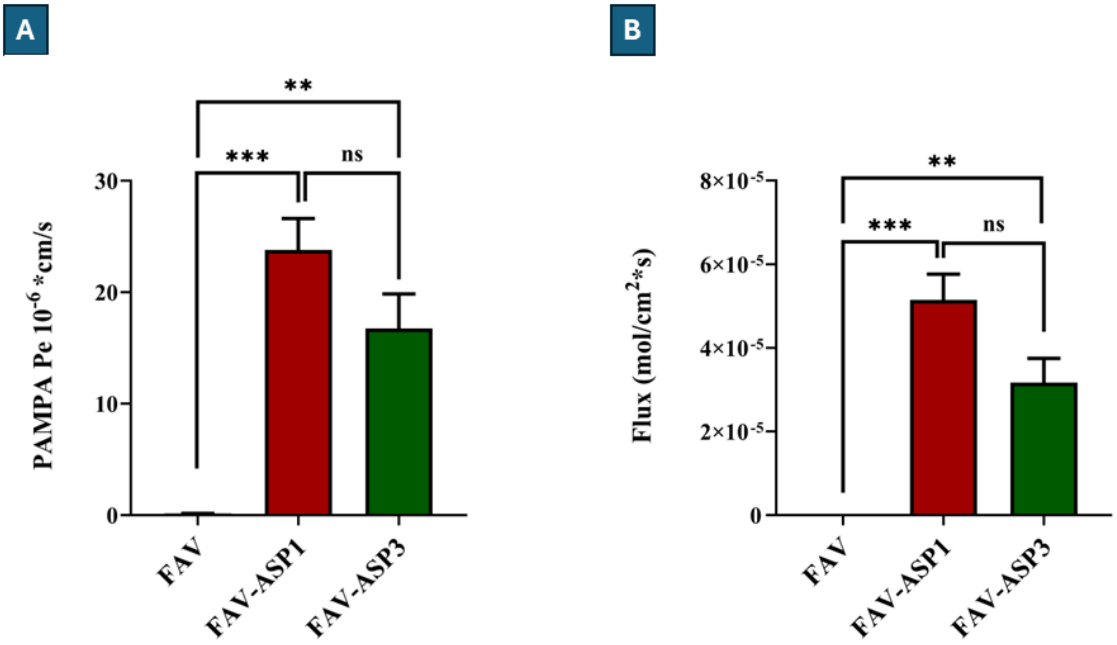

Figure 10. BBB-PAMPA results for FAV-ASP1, FAV-ASP3 in comparison with pure FAV. (A): permeability results, (B): flux results. Results are expressed as means ± SD (n = 6), (ns) means non-significant, **p-value < 0.01, and ***p-value < 0.001.

6.2.3. In vitro drug release at nasal conditions

The performance of FAV-ASP1 release at nasal conditions (pH 5.6) was evaluated in comparison to initial FAV, as shown in Figure 11. The result showed the FAV-ASP1 had a significantly higher cumulative release amount of FAV after 60 min in comparison to initial FAV (p-value < 0.001). This result could be attributed to the effect of AP, which reduces the surface tension, especially when integrated into a phospholipid monolayer [138]. Therefore, the integration of AP with CH and Span® 60 could effect on the fluidity of the vesicle membrane resulting in higher release rate.

Furthermore, the small particle size of the carrier increased the surface area and its hydrophilic properties.

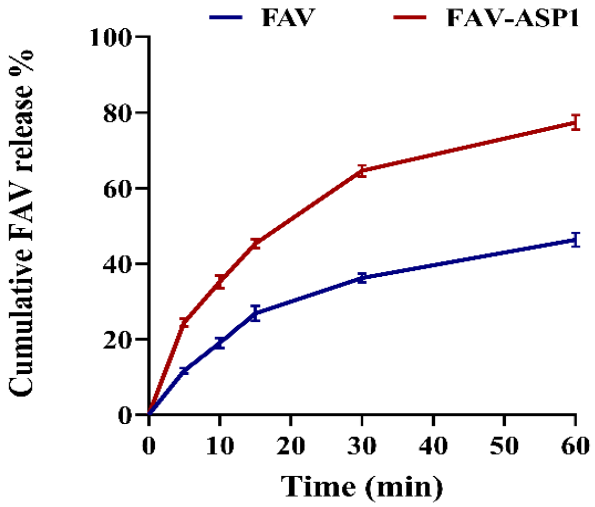

Figure 11. Cumulative *in vitro* release profile of FAV-ASP1 compared to pure FAV. Results are expressed as means ± SD (n = 3).

DDsolver® was used to evaluate the release kinetics for FAV-ASP1 at pH 5.6. The model with the highest R^2 value, with low AIC and the high MSC values is the best kinetics model (Table 8). The release profiles of FAV-ASP1 was fitted Korsmeyer-Peppas kinetic model, with release exponent "n" values of 0.44, indicating a quasi-Fickian diffusion (n < 0.45) [139].

Table 8. Comparison of release profiles (at SNES pH 5.6) using model dependent approaches

Model Parameters	Zero-order	First-order	Higuchi	Korsmeyer-Peppas
k	1.590	0.036	10.74	13.093
R^2	0.575	0.944	0.978	0.985
AIC	46.468	34.11	28.645	28.355
MSC	-0.029	2.030	2.941	2.989

Moreover, the evaluation of release profiles using model independent approaches demonstrated that FAV-ASP1 had higher AUC and DE values compared to initial FAV, as presented in Table 9. Additionally, FAV-ASP1 had a lower MDT value compared to initial FAV, indicating a faster release rate. Therefore, we can conclude that ASP vesicles could increase the absorption through the nasal cavity.

Table 9. Comparison of release profiles using model-independent approaches. Results are expressed as means ± SD (n = 3).

Sample	AUC (µg.min/mL)	DE (%)	MDT (min)
FAV	1922.26 ± 62.97	0.32 ± 0.01	18.48 ± 0.50
FAV-ASP1	3354.79 ± 49.43 [b]	0.55 ± 0.01 [b]	16.60 ± 0.45 [a]

Notes: [a] p-value < 0.001, [b] p-value <0.0001.

6.2.4. Rapid equilibrium dialysis measurement (RED)

To evaluate the release of FAV under blood conditions, we used RED. The result showed that the dissolution rate of FAV-ASP1 was increased by approximately 3.5-fold compared to pure FAV (p-value < 0.0001), which could be related to the nanosized particles and the effect of AP and Span® 60. As shown in Figure 12, the amount released of FAV increased rapidly during the first hour, and the equilibrium state of the formulation was reached after 2 h. This result could be related to the release of desorption FAV from the surface of the vesicles, followed by diffusion of FAV through the bilayers. Similar result obtained by Taymouri et al. (2016) [15].

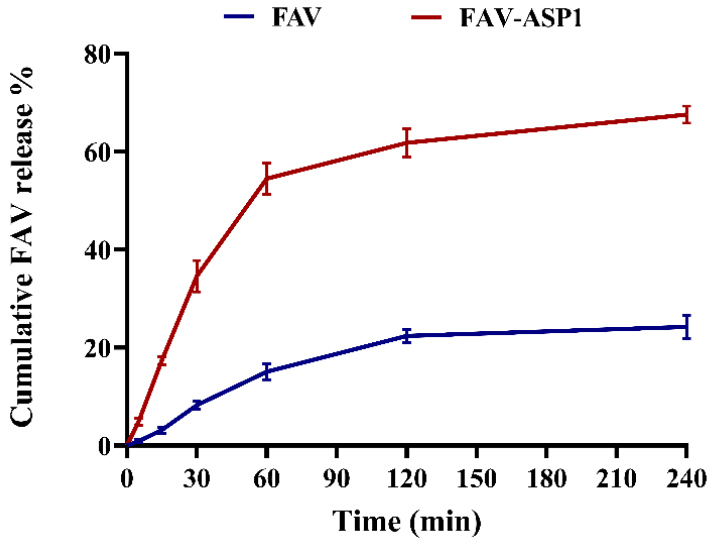

Figure 12. Rapid equilibrium dialysis (RED) of FAV-ASP1 in comparison with pure FAV. Results are expressed as means ± SD (n = 6).

6.2.5. Droplet size distribution measurement

Droplet size distribution is an important parameter for valuate the *in vitro* bioavailability and bioequivalence of liquid nasal formulations, and both the US FDA and EMA recommend its evaluation to ensure the suitability for spraying into the nasal cavity. Targeting the CNS requires

particle deposition in the posterior region of the nasal cavity (to reach the olfactory and trigeminal nerves) [140]. The recommended droplet size ranges between 20 to around 200 µm [141].

The results demonstrated that FAV-ASP1 was suitable for nasal administration (Dv50 = 174.80 ± 12.08 µm), which indicates a more posterior deposition; thus, increasing the absorption through the nasal cavity. Moreover, FAV-ASP1 showed small Span value, indicating a narrow width of droplet size distribution [142].

Table 10. Droplet size distribution results of FAV-ASP1. Results are presented as means ± SD (n = 3).

Formulation	Dv10 (µm)	Dv50 (µm)	Dv90 (µm)	Span (µm)
FAV-ASP8	61.07 ± 6.23	174.80 ± 12.08	500.50 ± 65.80	2.02 ± 0.86

6.2.6. Ex vivo nasal diffusion study on human nasal mucosa

As we mentioned previously, human nasal mucosa has been used to predict the absorption of the FAV-ASP formulation through the nasal cavity, and to predict the penetration across the BBB.

As shown in Figure 13, FAV-ASP1 had a significantly higher amount of FAV that permeated through the nasal mucosa compared to initial FAV within 60 min (1311.74 ± 41.70 µg/cm^2 and 128.17 ± 13.64 µg/cm^2, respectively), (p-value < 0.0001). This result demonstrates that using ASP as a drug carrier enhances drug absorption and permeation through the nasal mucosa, facilitating more efficient drug delivery via IN administration. The result could be attributed to the fact that nanoparticles smaller than 500 nm can pass through the aqueous, non-viscous pores of the mucin network, resulting in better penetration and absorption into the nasal epithelium. Additionally, the negative ZP helps to minimize the slow penetration by restricting contact with the negatively charged nasal membrane [143]. Moreover, AP has a surfactant-like property (like sorbitan derivatives), resulting in enhanced penetration.

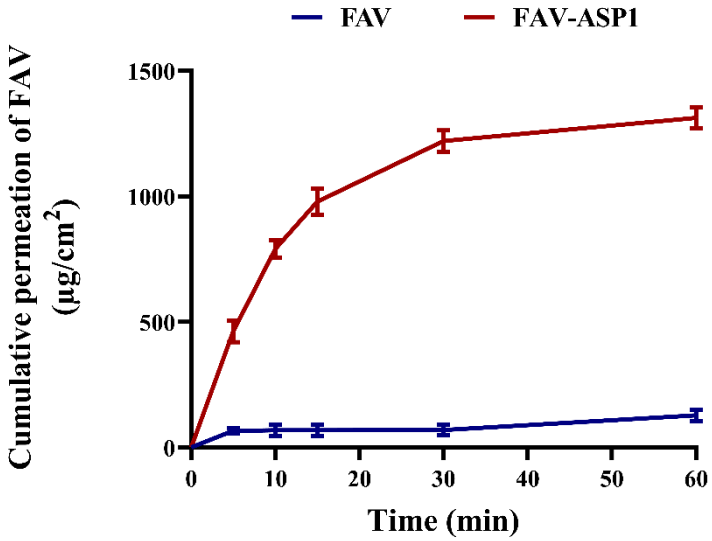

Figure 13. Ex vivo permeability study of FAV-ASP1 in comparison with initial FAV on human nasal mucosa. Results are expressed as means ± SD (n = 3).

The biopharmaceutical parameters, including steady-state flux (Jss), permeability coefficient (Kp) and enhancement ratio, were summarized in Table 11. The results indicated a significant enhancement in the biopharmaceutical parameters of FAV-ASP1 compared to initial FAV.

Table 11. The biopharmaceutical parameters of FAV-ASP1 compared to the initial FAV. Results are expressed as means ± SD (n = 3).

Sample	Flux (µg/cm²/h)	K_p (cm/h)	ER
FAV	2.13 ± 0.06	$0.002 \pm 7.12 \times 10^{-5}$	-
FAV-ASP1	21.86 ± 0.02 [a]	$0.011 \pm 1.45 \times 10^{-5}$ [a]	10.23 ± 0.28

Notes: [a] p-value < 0.0001.

6.2.7. Storage stability

The stability is an important parameter to evaluate the capacity of the drug carrier to resist environmental conditions, such as temperature, and for the protection of the encapsulated drug from degradation, thus determining the recommended storage conditions and the retest period for the formulation.

As shown in Figure 14A, FAV-ASP1 showed a significant decrease in Z-average values after 4 weeks (p-value < 0.0001), which could be attributed to changes in the mean intensity distribution

of particle sizes (Z-average is calculated by the intensity of the particle) [144]. On the other hand, the antioxidant properties of AP could be responsible for preventing oxidative degradation of the lipid bilayer, thereby maintaining vesicle integrity over time. FAV-ASP1 showed a non-significant change in PDI and ZP values over time (Figure 14B and 14C, respectively). Therefore, we can conclude that ASP vesicles were physically stable over time.

The evaluation of the chemical stability of FAV within the ASP vesicles demonstrated a significant decrease in FAV concentrations after 4 weeks (***p-value < 0.001), but the concentration was > 90% (92.94 ± 5.05 %), as shown in Figure 14D. Therefore, we can conclude that ASP vesicles improved the stability of FAV over time.

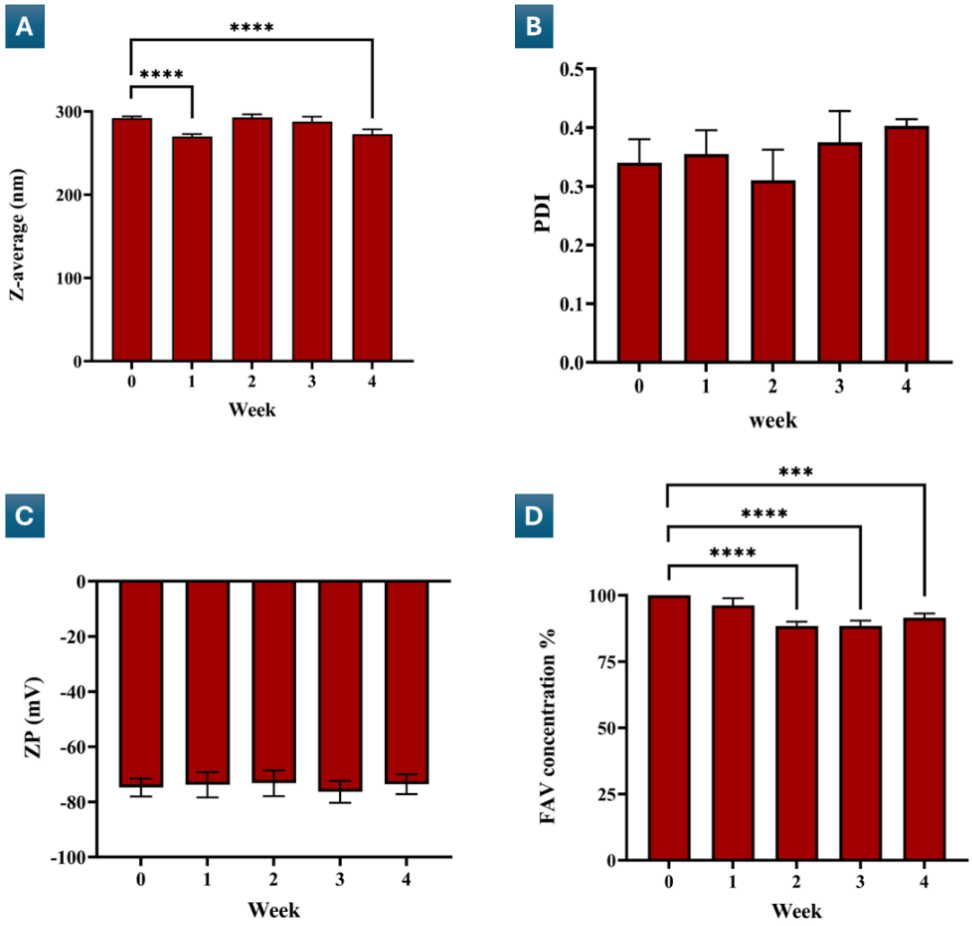

Figure 14. The stability results for 4 weeks at 4 °C; (A): Z-average variations, (B): PDI variations, (C): ZP variations, and (D): Concentration variations. ***p-value < 0.001, ****p-value <0.0001.

6.2.8. In vivo study

6.2.8.1. Evaluation of pharmacokinetic (PK) parameters

FAV has low water solubility (8.7 mg/mL) and limited permeability to the CNS, which can be attributed to its low passive permeability caused by the presence of three hydrogen bond donors [144]. The efficiency of formulations FAV-ASP1 to deliver FAV to the CNS after IN administration was tested using Sprague–Dawley rats.

The result demonstrated that FAV was successfully detected in the plasma (Figure 15), with a plasma concentration peak (Cmax) of 27.03 ± 6.88 and 26.24 ± 7.382 µg/mL at 7.5 ± 2.88 and 7.5 ± 2.88 min (T_{max}) after IN administration of FAV-ASP1 and initial FAV, respectively (as shown in Table 12).

Both FAV-ASP1 and initial FAV had the same T_{max}, which indicates that the similarity in the absorption rate. Moreover, FAV-ASP1 showed a higher half-life compared to the initial FAV (non-significant). FAV-ASP1 demonstrated a higher AUC0–t value, which reflects a higher actual body exposure to FAV after IN administration. The clearance values indicated that FAV-ASP1 had a slower elimination rate. The lower V_d value of FAV-ASP1 could mean a less distribution into tissues. However, FAV-ASP1 had a higher MRT value than the initial FAV, indicating a longer duration of FAV in the circulation system. As a result, FAV-ASP1 had a high relative bioavailability, indicating that ASP vesicles enhanced the bioavailability of FAV.

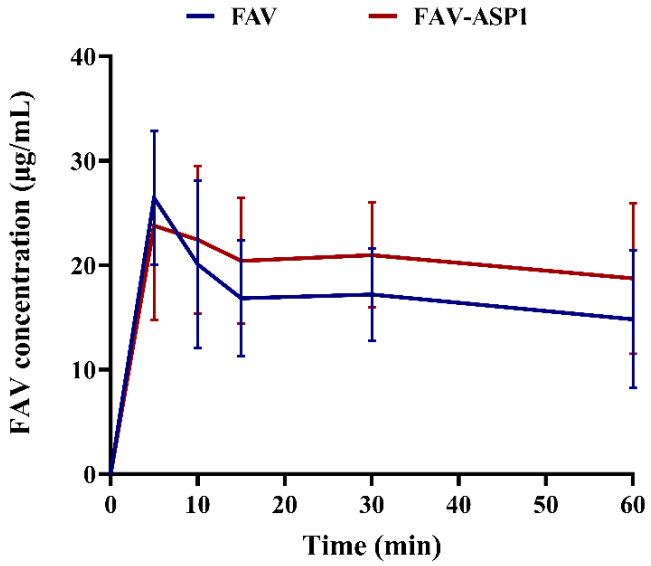

Figure 15. Plasma concentration–time profile after nasal administration of FAV-ASP1 and initial FAV in rats. Results are expressed as means ± SD (n = 4).

Table 11. Pharmacokinetic (PK) parameters of FAV-ASP1 and initial FAV after non-compartmental analysis. Results are expressed as means ± SD (n = 4).

PK parameters	FAV	FAV-ASP8
C_{max} (µg/mL)	26.24 ± 7.38	27.03 ± 6.88
T_{max} (min)	7.50 ± 2.88	7.50 ± 2.88
k_e (min^{-1})	0.007 ± 0.01	0.009 ± 0.005
$t_{1/2}$ (min)	127.54 ± 103.60	226.42 ± 337.06
AUC_{0-t} (µg × min/mL)	953.56 ± 282.31	1153.01 ± 364.87
$AUC_{0-\infty}$ (µg × min/mL)	4134.94 ± 4133.03	9305.40 ± 14438.56
C_L (mL/min)	0.88 ± 0.62	0.79 ± 0.56
V_d (mL)	104.57 ± 27.35	80.55 ± 19.01
MRT (min)	185.23 ± 153.68	329.96 ± 486.03
F (%)	-	124.53 ± 35.33

We evaluated the efficacy of ASP vesicles to deliver FAV to CNS by measuring the concentration of FAV in CSF samples after 1 h of the IN administration (Figure 16), where the olfactory nerve in the nasal cavity is considered a direct route to CNS, in addition to the direct link with the CSF in the subarachnoid space through the interstitial fluid surrounding the olfactory nerve bundle [53,145].

The result demonstrated that FAV was successfully reach the CSF, with a concentration of 8.29 ± 1.51 and 6.02 ± 1.04 µg/mL for FAV-ASP1 and initial FAV, respectively. The significant higher concentration of FAV-ASP1 (*p-value < 0.05) could be attributed to an increase in the extent of drug absorption through the nasal mucosa (olfactory nerves) due to the physical parameter, the lipophilicity nature of the vesicles and the presence of a permeation enhancer (Span® 60), which improves the membrane penetration. Furthermore, AP can overcome biological barriers, enter the brain and resist hydrolysis, thereby preventing the degradation of FAV. According to the chemical structure of FAV, amide hydrolysis and oxidation are the potential major degradation pathways [14].

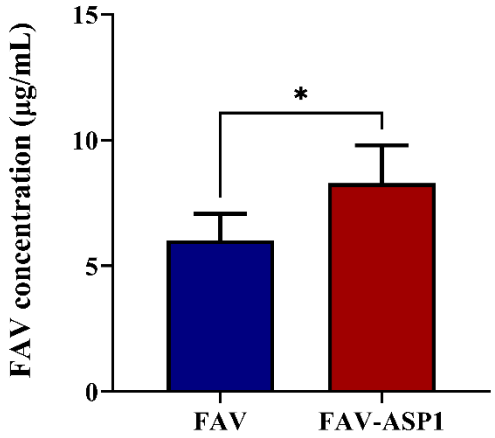

Figure 16. The concentration of FAV in cerebrospinal fluid (CSF) after 1 hour of nasal administration. Results are expressed as means ± SD (n = 4), *p-value < 0.05.

6.2.8.2. Evaluation of in vitro-in vivo correlations (IVIVC)

In this study, we used IVIVC to predict the *in vivo* performance of FAV-ASP1 based on its *in vitro* data. Figure 17 demonstrates the IVIVC graphs for the comparison of AUC_{0-t} values between the *in vitro* release and the *in vivo* PK data. The correlation coefficient (R^2) values were 0.971 and 0.982 for initial FAV and FAV-ASP1, respectively. Furthermore, R^2 values obtained from IVIVC graphs for the comparison of AUC_{0-t} values between the *in vitro* permeation and the *in vivo* PK data (Figure 18) showed a good point-to-point correlation (0.977 and 0.992 for initial FAV and FAV-ASP1, respectively). This result indicates that the use of in vitro release and permeation data to establish the IVIVC could be useful in predicting the in vivo properties of the formulations [14].

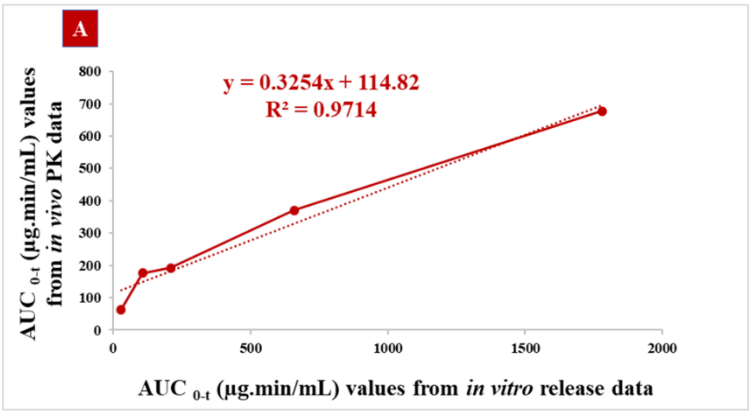

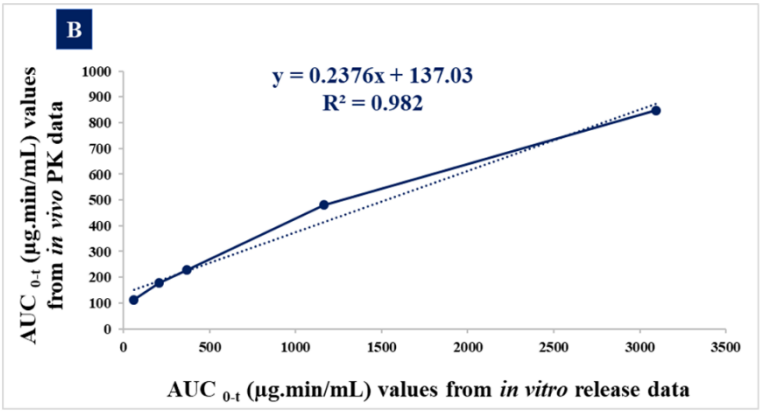

Figure 17. IVIVC graphs for the comparison of AUC $_{0\text{-}t}$ values between the in vitro release and the in vivo PK data. Where (A): IVIVC for initial FAV, (B): IVIVC for FAV-ASP1

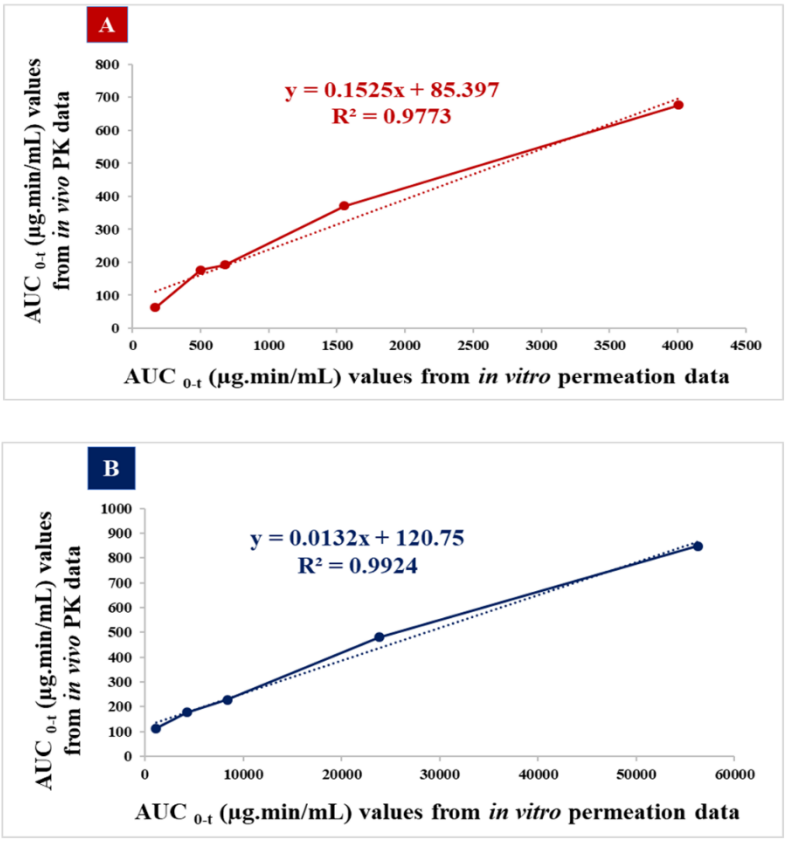

Figure 18. IVIVC graphs for the comparison of AUC $_{0\text{-}t}$ values between the *in vitro* permeation and the *in vivo* PK data. (A): IVIVC for initial FAV, (B): IVIVC for FAV-ASP1.

7. Conclusions

Nose-to-brain delivery system could be a promising strategy for targeting the CNS and overcome the bioavailability obstacles associated with oral administration such as poor solubility, first-pass hepatic metabolism, side effects and dose-dependent toxicity.

The composition of the nanocarriers plays crucial role in drug release and diffusion through the nasal mucosa, and bypassing BBB and BCSFB. Therefore, it is important to choose the appropriate nanocarriers.

In this Ph.D. work, we selected BSA nanoparticles as a carrier for LAM, and ASP as a carrier for FAV. Both nanocarriers showed excellent nasal applicability results, including article size, surface charge, mucoadhesion properties, and drug encapsulation.

The optimal LAM-BSA formulation demonstrated a higher cumulative release amount at blood conditions compared to nasal conditions, which could be related to the pH-dependent solubility of LAM. Moreover, the in vitro permeability results showed an improved in the flux value of LAM through the porcine brain polar lipid extract. The ex vivo permeability result illustrated a higher diffusion of LAM from LAM-BSA formulation through the human nasal mucosa compared to the initial LAM. Finally, the cell line studies demonstrated that the use of BSA as a carrier of LAM reduced its cytotoxicity and improved its permeability through Caco-2 cells.

On the other hand, the optimal FAV-ASP formulation showed enhancement in the stability and solubility of FAV, with a higher release rate under both nasal and blood circulation conditions. The in vitro permeability results showed higher permeability and flux values of FAV through the porcine brain polar lipid extract in comparison to initial FAV. Moreover, FAV-ASP formulation had a higher diffusion of FAV through the human nasal mucosa compared to the initial FAV. The in vivo study indicated that there was no significant difference in plasma concentrations for FAV-ASP in comparison to initial FAV, while it had a significantly higher CSF concentration. Additionally, IVIVC illustrated a good correlation between the in vitro and the in vivo PK data.

In summary, LAM-BSA and FAV-ASP could be a promising drug delivery systems for targeting the CNS, improve the bioavailability and reduce the adverse effects of the drugs.

8. Novelty and practical aspects

The conventional dosage forms for treating CNS disorders, including tablets, capsules, and injections, have several bioavailability challenges such as low solubility, poor absorption, physiological barriers, first-pass metabolism, and dose-dependent toxicity. Therefore, novel drug carriers and alternative routes of administration are required to overcome these obstacles, enhance the bioavailability and achieve therapeutic effects.

This Ph.D. work reported for the first time the use of BSA nanoparticles as a carrier for LAM, and ASP as a carrier for FAV.

Novel LAM-BSA and FAV-ASP formulations were optimized for nose-to-brain delivery system. These novel formulations improved the therapeutic effect and CNS targeting by:

- Achieving suitable drug carrier properties, including homogeneous nanosized particles (PDI < 0.5 and Z-average < 300 nm to cross the olfactory region and reach the CNS, and to improve the wettability and solubility), ZP > |±30 mV| (to ensure the physical stability, bypass BBB and escape from the reticuloendothelial system), good viscosity and mucoadhesion properties (to prolong the residence time on the nasal mucosa which improves the absorption and permeability through the nasal epithelium).
- Use a lower dose (2 mg/mL) comparing to oral administration; therefore, reduce the adverse effects of LAM and FAV; where the oral dose of LAM is 25 mg daily for two weeks, followed by an increase to 50 mg daily for two weeks, and for FAV is 1600 mg twice daily on day 1, followed by 600 mg twice daily on days 2 to 5.
- IN administration provides an appropriate alternative route to avoid the first-pass metabolism of LAM and FAV.
- BSA nanoparticles are useful to avoid the efflux of LAM by P-gp; therefore, reduce the dose-dependent toxicity of LAM.
- ASP vesicles improved the low CNS penetration of FAV, which associated with its low log P value (0.72).

9. Acknowledgment

Family first, always and forever. This PhD dissertation is a reflection of the unwavering love, support and encouragement of my family through this journey, which has been fraught with both professional and personal challenges. I owe an immense debt of gratitude to my parents for their endless love and sacrifices. For my brothers, my strength, I am deeply grateful for your belief in me and for lifting me during all challenges, especially Dr. Zain. For my niblings, my little angels, I love you all. For my niece, Meryam, you will always be my little daughter and my sunshine.

A heartfelt thank you to **Dr. Gábor Katona**, my supervisor, for your kindness, exceptional guidance, constant support, trust and motivation. I feel privileged to have your guidance and mentorship on this journey.

My sincere appreciation to my supervisor, **Prof. Dr. György Tibor Balogh**, for his constructive feedback and support that enhanced my PhD work and my academic journey.

Additionally, I would like to acknowledge **Prof. Dr. Ildikó Csóka**, the head of the Institute of Pharmaceutical Technology and Regulatory Affairs, and **Prof. Dr. Rita Ambrus** for providing the resources and facilities necessary to conduct my research.

I am equally thankful for **Prof. Dr. István Zupkó**, the head of the Institute of Pharmacodynamics and Biopharmacy, for the collaboration and contribution which made this research possible.

I would like to express my deep gratitude to everyone who contributed to the completion of this thesis: **Dr. Bence Sipos** and **Dr. Mária Budai-Szűcs** from Institute of Pharmaceutical Technology and Regulatory Affairs; **Dr. Zsuzsanna Schelz** from the Institute of Pharmacodynamics and Biopharmacy, University of Szeged; **Dr. István Lekli, Dr. István Bak, Alexandra Gyöngyösi** from the Department of Pharmacology, University of Debrecen; **Prof. Dr. Gábor Kozma and Prof. Dr. Zoltán Kónya** from the Department of Applied & Environmental Chemistry, University of Szeged; **Prof. Dr. László Rovó, Dr. Ágnes Szalenkó-Tőkés** and **Dr. Ágnes Kiricsi** from the Department of Oto-Rhino-Laryngology and Head-Neck Surgery, University of Szeged; **Dr. Diana Balogh-Weiser** from the Department of Physical Chemistry and Materials Science, Budapest University of Technology and Economics; and **Dr. Balázs Volk** from Egis Pharmaceuticals Plc.

I would like to extend my sincere thanks to my lab colleagues and the administrative and technical staff in the institute for their support and making this journey easier for me.

Finally, I must also express my deepest appreciation for my second family, for their unconditional love, encouragement and continuous support. To my supervisor in Syria, **Dr. Yousef Al-Ahmad** and his wife, **Ms. Nesreen Alkhadour**, for your friendship, for being always there for me in my

bad and good days and accepting me as a family member. To **Nawar Alkhadour,** I am grateful for having you here with me in this journey. To **Prof. Dr. Hala Deeb,** a heartfelt gratitude for the chance that led me to meet you, I cherish your presence in my life. To **Hanan Makhlof**, a friend in the sense of a sister, thank you for always being there for me. To **Shady Ashy**, my young brother, thank you for making me feel like a home away from home. To my friend for all times and memories, **Dr. Walaa Salamah**, thank you for standing by me. For who believed in me and supported me to pursue my academic journey, **Dr. Haifaa Al-Ali**, may your soul rest in peace.

To **Dr. Mahwash Mukhtar** and **Dr. Zsófia Németh**, for their friendship, motivation and willingness to listen, which have made this journey easier.

To my sustenance in life, the shoulder to cry on, my dear friends: **Dr. Suha Alnaeb, Lina Soliman, Lomass Soliman, Fatima Rajab, Hiba Alsoliman, Ola Salamah, Hanan Mohammad**, I am truly grateful for the strength you have given me.

To the gift of my life, the peace amidst chaos, and the light during my darkest days, thank you.

This PhD work was generously supported by the Stipendium Hungaricum Program, and by Project no. TKP2021-EGA-32 implemented with support provided by the Ministry of Culture and Innovation of Hungary from the National Research, Development and Innovation Fund, financed under the TKP2021-EGA funding scheme.

10. References

1. Steinmetz, J.D.; Maria Seeher, K.; Schiess, N.; Nichols, E.; Cao, B.; Servili, C.; Cavallera, V.; Cousin, E.; Hagins, H.; Moberg, M.E.; et al. Global, Regional, and National Burden of Disorders Affecting the Nervous System, 1990â€“2021: A Systematic Analysis for the Global Burden of Disease Study 2021. *Lancet Neurol* **2024**, *23*, 344–381, doi:10.1016/S1474-4422(24)00038-3.

2. Alotaibi, A.S.; Mahroos, R.A.; Yateem, S.S. Al; Menezes, R.G. Central Nervous System Causes of Sudden Unexpected Death: A Comprehensive Review. *Cureus* **2022**, *14*, e20944, doi:10.7759/CUREUS.20944.

3. Morofuji, Y.; Nakagawa, S. Drug Development for Central Nervous System Diseases Using In Vitro Blood-Brain Barrier Models and Drug Repositioning. *Curr Pharm Des* **2020**, *26*, 1466, doi:10.2174/1381612826666200224112534.

4. Musuc, M.; Salamah, M.; Budai-Sz, M.; Ucs, ″; Sipos, B.; Volk, B.; Katona, G.; Tibor Balogh, G.; Csóka, I. Development and Characterization of In Situ Gelling Nasal Cilostazol Spanlastics. *Gels 2025, Vol. 11, Page 82* **2025**, *11*, 82, doi:10.3390/GELS11020082.

5. Wohlfart, S.; Gelperina, S.; Kreuter, J. Transport of Drugs across the Blood–Brain Barrier by Nanoparticles. *Journal of Controlled Release* **2012**, *161*, 264–273, doi:10.1016/j.jconrel.2011.08.017.

6. Redzic, Z. Molecular Biology of the Blood-Brain and the Blood-Cerebrospinal Fluid Barriers: Similarities and Differences. *Fluids and Barriers of the CNS 2011 8:1* **2011**, *8*, 1–25, doi:10.1186/2045-8118-8-3.

7. Martins, P.P.; Smyth, H.D.C.; Cui, Z. Strategies to Facilitate or Block Nose-to-Brain Drug Delivery. *Int J Pharm* **2019**, *570*, 118635, doi:10.1016/j.ijpharm.2019.118635.

8. Trevino, J.T.; Quispe, R.C.; Khan, F.; Novak, V. Non-Invasive Strategies for Nose-to-Brain Drug Delivery. *J Clin Trials* **2020**, *10*, 439.

9. Asimakidou, E.; Tan, J.K.S.; Zeng, J.; Lo, C.H. Blood–Brain Barrier-Targeting Nanoparticles: Biomaterial Properties and Biomedical Applications in Translational Neuroscience. *Pharmaceuticals 2024, Vol. 17, Page 612* **2024**, *17*, 612, doi:10.3390/PH17050612.

10. Kakinen, A.; Jiang, Y.; Davis, T.P.; Teesalu, T.; Saarma, M. Brain Targeting Nanomedicines: Pitfalls and Promise. *Int J Nanomedicine* **2024**, *19*, 4857–4875, doi:10.2147/IJN.S454553.

11. Seju, U.; Kumar, A.; Sawant, K.K. Development and Evaluation of Olanzapine-Loaded PLGA Nanoparticles for Nose-to-Brain Delivery: In Vitro and in Vivo Studies. *Acta Biomater* **2011**, *7*, 4169–4176, doi:10.1016/J.ACTBIO.2011.07.025.

12. Yokel, R.A. Direct Nose to the Brain Nanomedicine Delivery Presents a Formidable Challenge. *Wiley Interdiscip Rev Nanomed Nanobiotechnol* **2022**, *14*, doi:10.1002/WNAN.1767.

13. Lee, D.; Minko, T. Nanotherapeutics for Nose-to-Brain Drug Delivery: An Approach to Bypass the Blood Brain Barrier. *Pharmaceutics* **2021**, *13*, doi:10.3390/PHARMACEUTICS13122049.

14. Formica, M.L.; Real, D.A.; Picchio, M.L.; Catlin, E.; Donnelly, R.F.; Paredes, A.J. On a Highway to the Brain: A Review on Nose-to-Brain Drug Delivery Using Nanoparticles. *Appl Mater Today* **2022**, *29*, 101631, doi:10.1016/j.apmt.2022.101631.

15. Salamah, M.; Volk, B.; Lekli, I.; Bak, I.; Gyöngyösi, A.; Kozma, G.; Kónya, Z.; Szalenkó-Tőkés, Á.; Kiricsi, Á.; Rovó, L.; et al. Preparation, and Ex Vivo and in Vivo Characterization of Favipiravir-Loaded Aspasomes and Niosomes for Nose-to-Brain Administration. *Int J Nanomedicine* **2025**, *20*, 6489–6514, doi:10.2147/IJN.S518486.

16. Salamah, M.; Sipos, B.; Schelz, Z.; Zupkó, I.; Kiricsi, Á.; Szalenkó-Tőkés, Á.; Rovó, L.; Katona, G.; Balogh, G.T.; Csóka, I. Development, in Vitro and Ex Vivo Characterization of Lamotrigine-Loaded Bovine Serum Albumin Nanoparticles Using QbD Approach. *Drug Deliv* **2025**, *32*, doi:10.1080/10717544.2025.2460693.

17. Rai, G.; Sharma, S.; Bhasin, J.; Aggarwal, K.; Ahuja, A.; Dang, S. Nanotechnological Advances in the Treatment of Epilepsy: A Comprehensive Review. *Nanotechnology* **2024**, *35*, 152002, doi:10.1088/1361-6528/AD1C95.

18. Manole, A.; Sirbu, C.; Mititelu, M.; Vasiliu, O.; Lorusso, L.; Sirbu, O.; Ionita Radu, F. State of the Art and Challenges in Epilepsy—A Narrative Review. *JPM* **2023**, *13*, 623, doi:10.3390/jpm13040623.

19. Bekbolatova, M.; Mayer, J.; Jose, R.; Syed, F.; Kurgansky, G.; Singh, P.; Pao, R.; Zaw, H.; Devine, T.; Chan-Akeley, R.; et al. Biomechanical Effects of Seizures on Cerebral Dynamics and Brain Stress. *Brain Sciences 2024, Vol. 14, Page 323* **2024**, *14*, 323, doi:10.3390/BRAINSCI14040323.

20. Holsti, M.; Dudley, N.; Schunk, J.; Adelgais, K.; Greenberg, R.; Olsen, C.; Healy, A.; Firth, S.; Filloux, F. Intranasal Midazolam vs Rectal Diazepam for the Home Treatment of Acute Seizures in Pediatric Patients with Epilepsy. *Arch Pediatr Adolesc Med* **2010**, *164*, 747–753, doi:10.1001/ARCHPEDIATRICS.2010.130.

21. Mohsen, A.M.; Salama, A.A.A.; Asfour, M.H. Cubosome-Based Thermosensitive in Situ Gelling System for Intranasal Administration of Lamotrigine with Enhanced Antiepileptic Efficacy. *Pharm Dev Technol* **2023**, *28*, 520–534, doi:10.1080/10837450.2023.2216755.

22. Gangurde, P.K.; Ajitkumar B, N.; Kumar, L. Lamotrigine Lipid Nanoparticles for Effective Treatment of Epilepsy: A Focus on Brain Targeting via Nasal Route. *Journal of Pharmaceutical Innovation 2018 14:2* **2018**, *14*, 91–111, doi:10.1007/S12247-018-9343-Z.

23. Zhang, D.D.; Wang, Z.Y.; Zhang, Y.R.; Gao, P.Y.; Zhang, W.; Fu, Y.; Chi, H.C.; Ma, L.Y.; Ge, Y.J.; He, X.Y.; et al. Epilepsy and Brain Health: A Large Prospective Cohort Study. *J Transl Med* **2024**, *22*, 1–14, doi:10.1186/S12967-024-06006-9/FIGURES/5.

24. Sumadewi, K.T.; Harkitasari, S.; Tjandra, D.C. Biomolecular Mechanisms of Epileptic Seizures and Epilepsy: A Review. *Acta Epileptologica* **2023**, *5*, 1–22, doi:10.1186/S42494-023-00137-0/TABLES/1.

25. Löscher, W.; Howe, C.L. Molecular Mechanisms in the Genesis of Seizures and Epilepsy Associated With Viral Infection. *Front Mol Neurosci* **2022**, *15*, 870868, doi:10.3389/FNMOL.2022.870868/XML/NLM.

26. Nath, A.; Tyler, K.L. Novel Approaches and Challenges to Treatment of Central Nervous System Viral Infections. *Ann Neurol* **2013**, *74*, 412, doi:10.1002/ANA.23988.

27. Abeywickrema, M.; Kelly, D.; Kadambari, S. Management of Neonatal Central Nervous System Viral Infections: Knowledge Gaps and Research Priorities. *Rev Med Virol* **2023**, *33*, e2421, doi:10.1002/RMV.2421.

28. Yachou, Y.; El Idrissi, A.; Belapasov, V.; Ait Benali, S. Neuroinvasion, Neurotropic, and Neuroinflammatory Events of SARS-CoV-2: Understanding the Neurological Manifestations in COVID-19 Patients. *Neurological Sciences* **2020**, *41*, 2657, doi:10.1007/S10072-020-04575-3.

29. Löscher, W. Epilepsy and Alterations of the Blood–Brain Barrier: Cause or Consequence of Epileptic Seizures or Both? *Handb Exp Pharmacol* **2022**, *273*, 331–350, doi:10.1007/164_2020_406/FIGURES/2.

30. Löscher, W.; Friedman, A. Structural, Molecular, and Functional Alterations of the Blood-Brain Barrier during Epileptogenesis and Epilepsy: A Cause, Consequence, or Both? *Int J Mol Sci* **2020**, *21*, 591, doi:10.3390/IJMS21020591.

31. Chen, T.S.; Huang, T.H.; Lai, M.C.; Huang, C.W. The Role of Glutamate Receptors in Epilepsy. *Biomedicines* **2023**, *11*, 783, doi:10.3390/BIOMEDICINES11030783.

32. Bauer, B.; Hartz, A.M.S.; Pekcec, A.; Toellner, K.; Miller, D.S.; Potschka, H. Seizure-Induced Up-Regulation of P-Glycoprotein at the Blood-Brain Barrier through Glutamate and Cyclooxygenase-2 Signaling. *Mol Pharmacol* **2008**, *73*, 1444–1453, doi:10.1124/MOL.107.041210.

33. Shah, P.; Dubey, P.; Vyas, B.; Kaul, A.; Mishra, A.K.; Chopra, D.; Patel, P. Lamotrigine Loaded PLGA Nanoparticles Intended for Direct Nose to Brain Delivery in Epilepsy: Pharmacokinetic, Pharmacodynamic and Scintigraphy Study. *Artif Cells Nanomed Biotechnol* **2021**, *49*, 511–522, doi:10.1080/21691401.2021.1939709.

34. Singh, J.; Garg, R.; Gupta, G. Das Enhancement of Solubility of Lamotrigine by Solid Dispersion and Development of Orally Disintegrating Tablets Using 3 ^2 Full Factorial Design. *J Pharm (Cairo)* **2015**, *2015*, 1–8, doi:10.1155/2015/828453.

35. Abdelmonem, R.; El-Enin, H.A.A.; Abdelkader, G.; Abdel-Hakeem, M. Formulation and Characterization of Lamotrigine Nasal Insert Targeted Brain for Enhanced Epilepsy Treatment. *Drug Deliv* **2023**, *30*, 2163321, doi:10.1080/10717544.2022.2163321.

36. Betchel, N.T.; Fariba, K.A.; Saadabadi, A. Lamotrigine. *The Essence of Analgesia and Analgesics* **2023**, 306–309, doi:10.1017/CBO9780511841378.074.

37. Costa, B.; Vale, N. Understanding Lamotrigine's Role in the CNS and Possible Future Evolution. *Int J Mol Sci* **2023**, *24*, 6050, doi:10.3390/IJMS24076050.

38. Liu, J.S.; Wang, J.H.; Zhou, J.; Tang, X.H.; Lan, X.; Shen, T.; Wu, X.Y.; Hong, Z. Enhanced Brain Delivery of Lamotrigine with Pluronic® P123-Based Nanocarrier. *Int J Nanomedicine* **2014**, *9*, 3923–3935, doi:10.2147/IJN.S62263.

39. Sources of Lamotrigine Pharmacokinetic Variability_ A Systematic Review of Population Pharmacokinetic Analyses | Enhanced Reader (accessed on 9 July 2025).

40. Nigam, K.; Kaur, A.; Tyagi, A.; Nematullah, M.; Khan, F.; Gabrani, R.; Dang, S. Nose-to-Brain Delivery of Lamotrigine-Loaded PLGA Nanoparticles. *Drug Deliv. and Transl. Res.* **2019**, *9*, 879–890, doi:10.1007/s13346-019-00622-5.

41. Anjali, P.B.; Jawahar, N.; Praharsh Kumar, M.R.; Jubie, S.; Selvamuthukumar, S. Nanocarriers in the Treatment of Epilepsy: Challenges and Opportunities. *J Drug Deliv Sci Technol* **2024**, *97*, 105788, doi:10.1016/J.JDDST.2024.105788.

42. Kausar, S.; Said Khan, F.; Ishaq Mujeeb Ur Rehman, M.; Akram, M.; Riaz, M.; Rasool, G.; Hamid Khan, A.; Saleem, I.; Shamim, S.; Malik, A. A Review: Mechanism of Action of Antiviral Drugs. *Int J Immunopathol Pharmacol* **2021**, *35*, 20587384211002620, doi:10.1177/20587384211002621.

43. Sun, M.; Manson, M.L.; Guo, T.; de Lange, E.C.M. CNS Viral Infections—What to Consider for Improving Drug Treatment: A Plea for Using Mathematical Modeling Approaches. *CNS Drugs 2024 38:5* **2024**, *38*, 349–373, doi:10.1007/S40263-024-01082-3.

44. Moshikur, R.M.; Ali, M.K.; Wakabayashi, R.; Moniruzzaman, M.; Goto, M. Favipiravir-Based Ionic Liquids as Potent Antiviral Drugs for Oral Delivery: Synthesis, Solubility, and Pharmacokinetic Evaluation. *Mol Pharm* **2021**, *18*, 3108–3115, doi:10.1021/ACS.MOLPHARMACEUT.1C00324/ASSET/IMAGES/LARGE/MP1C00324_0007.JPEG.

45. Vemuri, D.K.; Gundla, R.; Konduru, N.; Mallavarapu, R.; Katari, N.K. Favipiravir (SARS-CoV-2) Degradation Impurities: Identification and Route of Degradation Mechanism in the Finished Solid Dosage Form Using LC/LC–MS Method. *Biomedical Chromatography* **2022**, *36*, e5363, doi:10.1002/BMC.5363.

46. Sajadian, S.A.; Ardestani, N.S.; Esfandiari, N.; Askarizadeh, M.; Jouyban, A. Solubility of Favipiravir (as an Anti-COVID-19) in Supercritical Carbon Dioxide: An Experimental Analysis and Thermodynamic Modeling. *J Supercrit Fluids* **2022**, *183*, 105539, doi:10.1016/J.SUPFLU.2022.105539.

47. Moolasart, V.; Wongsawat, J.; Phokhom, P.; Thienthong, V. Favipiravir-Based Regimen for Coronavirus Disease 2019 Pneumonia for a 47-Day-Old Male Newborn. *SAGE Open Med Case Rep* **2020**, *8*, 2050313X20964046, doi:10.1177/2050313X20964046.

48. Joshi, S.; Parkar, J.; Ansari, A.; Vora, A.; Talwar, D.; Tiwaskar, M.; Patil, S.; Barkate, H. Role of Favipiravir in the Treatment of COVID-19. *International Journal of Infectious Diseases* **2021**, *102*, 501–508, doi:10.1016/j.ijid.2020.10.069.

49. Hayden, F.G.; Lenk, R.P.; Epstein, C.; Kang, L.L. Oral Favipiravir Exposure and Pharmacodynamic Effects in Adult Outpatients With Acute Influenza. *J Infect Dis* **2024**, *230*, e395–e404, doi:10.1093/INFDIS/JIAD409.

50. Eryildiz-Yesir, B.; Ozgun, H.; Ersahin, M.E.; Rajabi, H.R.; Vatanpour, V.; Koyuncu, I. Degradation of Antiviral Drug Favipiravir Using UV, UV/H2O2, and Photocatalysis with Co-Doped ZnS Quantum Dots: Operational Parameters, Kinetic Studies, and Toxicity Assessment. *Langmuir* **2025**, *41*, 6528–6543, doi:10.1021/ACS.LANGMUIR.4C03639/ASSET/IMAGES/LARGE/LA4C03639_0013.JPEG.

51. Pilkington, V.; Pepperrell, T.; Hill, A. A Review of the Safety of Favipiravir – a Potential Treatment in the COVID-19 Pandemic? *J Virus Erad* **2020**, *6*, 45, doi:10.1016/S2055-6640(20)30016-9.

52. Samanta, D. Rescue Therapies for Seizure Emergencies: Current and Future Landscape. *Neurological Sciences* **2021**, *42*, 4017–4027, doi:10.1007/S10072-021-05468-9/TABLES/2.

53. Singh, R.; Gulani, M.; Vijayanand, S.; Arte, T.; Adediran, E.; Pasupuleti, D.; Patel, P.; Ferguson, A.; Uddin, M.; Zughaier, S.M.; et al. An Intranasal Quadruple Variant Vaccine Approach Using SARS-CoV-2 and Influenza A: Delta, Omicron, H1N1and H3N2. **2025**, doi:10.1016/j.ijpharm.2025.126043.

54. Huang, Q.; Chen, X.; Yu, S.; Gong, G.; Shu, H. Research Progress in Brain-Targeted Nasal Drug Delivery. *Front Aging Neurosci* **2023**, *15*, 1341295, doi:10.3389/FNAGI.2023.1341295/BIBTEX.

55. Gandhi, S.; Shastri, D.H.; Shah, J.; Nair, A.B.; Jacob, S. Nasal Delivery to the Brain: Harnessing Nanoparticles for Effective Drug Transport. *Pharmaceutics* **2024**, *16*, 481, doi:10.3390/pharmaceutics16040481.

56. Djupesland, P.G.; Messina, J.C.; Mahmoud, R.A. The Nasal Approach to Delivering Treatment for Brain Diseases: An Anatomic, Physiologic, and Delivery Technology Overview. *Ther Deliv* **2014**, *5*, 709–733, doi:10.4155/TDE.14.41.

57. Chen, M.; Pekosz, A.; Villano, J.S.; Shen, W.; Zhou, R.; Kulaga, H.; Li, Z.; Smith, A.; Gurung, A.; Beck, S.E.; et al. Evolution of Nasal and Olfactory Infection Characteristics of SARS-CoV-2 Variants. *J Clin Invest* **2024**, *134*, e174439, doi:10.1172/JCI174439.

58. Alam, T.; Pandit, J.; Vohora, D.; Aqil, M.; Ali, A.; Sultana, Y. Optimization of Nanostructured Lipid Carriers of Lamotrigine for Brain Delivery: In Vitro Characterization and in Vivo Efficacy in Epilepsy. *Expert Opin Drug Deliv* **2015**, *12*, 181–194, doi:10.1517/17425247.2014.945416.

59. Drath, I.; Richter, F.; Feja, M. Nose-to-Brain Drug Delivery: From Bench to Bedside. *Translational Neurodegeneration 2025 14:1* **2025**, *14*, 1–22, doi:10.1186/S40035-025-00481-W.

60. Drath, I.; Richter, F.; Feja, M. Nose-to-Brain Drug Delivery: From Bench to Bedside. *Translational Neurodegeneration 2025 14:1* **2025**, *14*, 1–22, doi:10.1186/S40035-025-00481-W.

61. Shen, H.; Aggarwal, N.; Cui, B.; Foo, G.W.; He, Y.; Srivastava, S.K.; Li, S.; Seah, M.Z.X.; Wun, K.S.; Ling, H.; et al. Engineered Commensals for Targeted Nose-to-Brain Drug Delivery. *Cell* **2025**, *188*, 1545-1562.e16, doi:10.1016/J.CELL.2025.01.017.

62. Sailer, M.M.; Köllmer, M.; Masson, B.; Fais, F.; Hohenfeld, I.P.; Herbig, M.E.; Koitschev, A.K.; Becker, S. Nasal Residence Time and Rheological Properties of a New Bentonite-Based Thixotropic Gel Emulsion Nasal Spray – AM-301. *Drug Dev Ind Pharm* **2023**, *49*, 103–114, doi:10.1080/03639045.2023.2183724.

63. Kisku, A.; Nishad, A.; Agrawal, S.; Paliwal, R.; Datusalia, A.K.; Gupta, G.; Singh, S.K.; Dua, K.; Sulakhiya, K. Recent Developments in Intranasal Drug Delivery of Nanomedicines for the Treatment of Neuropsychiatric Disorders. *Front Med (Lausanne)* **2024**, *11*, 1463976, doi:10.3389/FMED.2024.1463976/XML.

64. Agu, R.U.; Ugwoke, M.I. In Situ and Ex Vivo Nasal Models for Preclinical Drug Development Studies. *Drug Absorption Studies* **2007**, 112–134, doi:10.1007/978-0-387-74901-3_5.

65. Mittal, V.; Yadav, K.S. Optimizing Nasal Drug Delivery for Peptides, Proteins, and Small Molecules: Strategic Use of Materials and Techniques to Target the CNS. *International Journal of Polymeric Materials and Polymeric Biomaterials* **2025**, doi:10.1080/00914037.2024.2443165.

66. Nigam, K.; Kaur, A.; Tyagi, A.; Manda, K.; Goswami, N.; Nematullah, M.; Khan, F.; Gabrani, R.; Gauba, P.; Dang, S. In Vitro & in Vivo Evaluations of PLGA Nanoparticle Based Combinatorial Drug Therapy for Baclofen and Lamotrigine for Neuropathic Pain Management. *J Microencapsul* **2022**, *39*, 95–109, doi:10.1080/02652048.2022.2041751.

67. McNamara, K.; Tofail, S.A.M. Nanoparticles in Biomedical Applications. *Adv Phys X* **2017**, *2*, 54–88, doi:10.1080/23746149.2016.1254570.

68. Liu, J.; Wang, T.; Dong, J.; Lu, Y. The Blood–Brain Barriers: Novel Nanocarriers for Central Nervous System Diseases. *Journal of Nanobiotechnology 2025 23:1* **2025**, *23*, 1–29, doi:10.1186/S12951-025-03247-8.

69. Katona, G.; Balogh, G.T.; Dargó, G.; Gáspár, R.; Márki, Á.; Ducza, E.; Sztojkov-Ivanov, A.; Tömösi, F.; Kecskeméti, G.; Janáky, T.; et al. Development of Meloxicam-Human Serum Albumin Nanoparticles for Nose-to-Brain Delivery via Application of a Quality by Design Approach. *Pharmaceutics* **2020**, *12*, 97, doi:10.3390/pharmaceutics12020097.

70. Tartari, A.P.S.; Peczek, S.H.; Fin, M.T.; Ziebarth, J.; Machado, C.S.; Mainardes, R.M. Bovine Serum Albumin Nanoparticles Enhanced the Intranasal Bioavailability of Silybin in Rats. *Pharmaceutics* **2023**, *15*, doi:10.3390/PHARMACEUTICS15122648.

71. Awad, R.; Avital, A.; Sosnik, A. Polymeric Nanocarriers for Nose-to-Brain Drug Delivery in Neurodegenerative Diseases and Neurodevelopmental Disorders. *Acta Pharm Sin B* **2023**, *13*, 1866–1886, doi:10.1016/J.APSB.2022.07.003.

72. Gadhave, D.G.; Kokare, C.R. Nanostructured Lipid Carriers Engineered for Intranasal Delivery of Teriflunomide in Multiple Sclerosis: Optimization and in Vivo Studies. *Drug Dev Ind Pharm* **2019**, *45*, 839–851, doi:10.1080/03639045.2019.1576724.

73. Song, Y.; Li, N.; Luo, Q.; Liu, D.; Wang, Z. Intranasal Administrations of AP39-Loaded Liposomes Selectively Deliver H2S to Neuronal Mitochondria to Protect Neonatal Hypoxia-Ischemia by Targeting ERK1/2 and Caspase-1. *ACS Biomater Sci Eng* **2025**, doi:10.1021/ACSBIOMATERIALS.4C02282/SUPPL_FILE/AB4C02282_SI_001.PDF.

74. Patil, V.S.; Sutar, K.P.; Pockle, R.D.; Usulkar, S.; Jadhav, V.A. Formulation, Optimization and Evaluation of Amisulpride-Loaded Niosomal Intranasal Gel for Brain Targeting. *Ther Deliv* **2023**, *14*, 635–647, doi:10.4155/TDE-2023-0059.

75. Correia, A.C.; Monteiro, A.R.; Silva, R.; Moreira, J.N.; Sousa Lobo, J.M.; Silva, A.C. Lipid Nanoparticles Strategies to Modify Pharmacokinetics of Central Nervous System Targeting Drugs: Crossing or Circumventing the Blood–Brain Barrier (BBB) to Manage Neurological Disorders. *Adv Drug Deliv Rev* **2022**, *189*, 114485, doi:10.1016/J.ADDR.2022.114485.

76. Moribe, K.; Limwikrant, W.; Higashi, K.; Yamamoto, K. Drug Nanoparticle Formulation Using Ascorbic Acid Derivatives. *J Drug Deliv* **2011**, *2011*, 1–9, doi:10.1155/2011/138929.

77. Palma, S.; Manzo, R.; Lo Nostro, P.; Allemandi, D. Nanostructures from Alkyl Vitamin C Derivatives (ASCn): Properties and Potential Platform for Drug Delivery. *Int J Pharm* **2007**, *345*, 26–34, doi:10.1016/J.IJPHARM.2007.09.014.

78. Gopinath, D.; Ravi, D.; Rao, B.R.; Apte, S.S.; Renuka, D.; Rambhau, D. Ascorbyl Palmitate Vesicles (Aspasomes): Formation, Characterization and Applications. *Int J Pharm* **2004**, *271*, 95–113, doi:10.1016/j.ijpharm.2003.10.032.

79. Khalil, R.M.; Abdelbary, A.; Arini, S.K. El; Basha, M.; El-Hashemy, H.A.; Farouk, F. Development of Tizanidine Loaded Aspasomes as Transdermal Delivery System: Ex-Vivo and in-Vivo Evaluation. *J Liposome Res* **2021**, *31*, 19–29, doi:10.1080/08982104.2019.1684940.

80. Han, S. Structure of Ascorbyl Palmitate Bilayers (Aspasomes) from Molecular Dynamics Simulation. *Bull Korean Chem Soc* **2018**, *39*, 887–890, doi:10.1002/BKCS.11475.

81. Rahimnejad, M.; Najafpour, G.; Bakeri, G. Investigation and Modeling Effective Parameters Influencing the Size of BSA Protein Nanoparticles as Colloidal Carrier. *Colloids Surf A Physicochem Eng Asp* **2012**, *412*, 96–100, doi:10.1016/j.colsurfa.2012.07.022.

82. Rohiwal, S.S.; Satvekar, R.K.; Tiwari, A.P.; Raut, A. V; Kumbhar, S.G.; Pawar, S.H. Investigating the Influence of Effective Parameters on Molecular Characteristics of Bovine Serum Albumin Nanoparticles. *Appl Surf Sci* **2015**, *334*, 157–164, doi:10.1016/j.apsusc.2014.08.170.

83. Yang, C.; Di, P.; Fu, J.; Xiong, H.; Jing, Q.; Ren, G.; Tang, Y.; Zheng, W.; Liu, G.; Ren, F. Improving the Physicochemical Properties of Bicalutamide by Complex Formation with Bovine Serum Albumin. *European Journal of Pharmaceutical Sciences* **2017**, *106*, 381–392, doi:10.1016/j.ejps.2017.05.059.

84. Chen, B.; Wu, C.; Zhuo, R.X.; Cheng, S.X. A Self-Assembled Albumin Based Multiple Drug Delivery Nanosystem to Overcome Multidrug Resistance. *RSC Adv* **2014**, *5*, 6807–6814, doi:10.1039/C4RA12802H.

85. Hassanin, I.; Elzoghby, A. Albumin-Based Nanoparticles: A Promising Strategy to Overcome Cancer Drug Resistance. *Cancer Drug Resist 2020;3:930-46.* **2020**, *3*, 930–946, doi:10.20517/CDR.2020.68.

86. Malaiya, A.; Kenwat, R.; Mamgain, A.; Nayak, P.; Parker, A.; Paliwal, S.R.; Paliwal, R. Intranasal Resveratrol Delivery to the Brain with Chitosan-Decorated Bovine Serum Albumin

Nanoparticles: Advancing Alzheimer's Management in Old Female Rats through QbD-Based Optimization, in Vitro Evaluation, and in Vivo Exploration. *Int J Biol Macromol* **2025**, *311*, 143300, doi:10.1016/J.IJBIOMAC.2025.143300.

87. Tavano, L.; Muzzalupo, R.; Trombino, S.; Cassano, R.; Pingitore, A.; Picci, N. Effect of Formulations Variables on the in Vitro Percutaneous Permeation of Sodium Diclofenac from New Vesicular Systems Obtained from Pluronic Triblock Copolymers. *Colloids Surf B Biointerfaces* **2010**, *79*, 227–234, doi:10.1016/j.colsurfb.2010.03.055.

88. Peng, W.; Jiang, X.Y.; Zhu, Y.; Omari-Siaw, E.; Deng, W.W.; Yu, J.N.; Xu, X.M.; Zhang, W.M. Oral Delivery of Capsaicin Using MPEG-PCL Nanoparticles. *Acta Pharmacol Sin* **2015**, *36*, 139–148, doi:10.1038/APS.2014.113.

89. Zhang, Y.; Huo, M.; Zhou, J.; Zou, A.; Li, W.; Yao, C.; Xie, S. DDSolver: An Add-In Program for Modeling and Comparison of Drug Dissolution Profiles. *AAPS J* **2010**, *12*, 263, doi:10.1208/S12248-010-9185-1.

90. JPPRes In Vitro Pharmaco-Equivalence Analysis of Diclofenac Potassium Oral Film-Coated Tablet Relative to Marketed Generics. **2023**, doi:10.56499/jppres23.1641_11.4.585.

91. Abdul Rasool, B.K.; Mohammed, A.A.; Salem, Y.Y. The Optimization of a Dimenhydrinate Transdermal Patch Formulation Based on the Quantitative Analysis of in Vitro Release Data by DDSolver through Skin Penetration Studies. *Sci Pharm* **2021**, *89*, 33, doi:10.3390/SCIPHARM89030033/S1.

92. Pascoal, A.D.S.M.R.; da Silva, P.M.; Coelho Pinheiro, M.N. Drug Dissolution Profiles from Polymeric Matrices: Data versus Numerical Solution of the Diffusion Problem and Kinetic Models. *International Communications in Heat and Mass Transfer* **2015**, *61*, 118–127, doi:10.1016/J.ICHEATMASSTRANSFER.2014.12.011.

93. Katona, G.; Sabir, F.; Sipos, B.; Naveed, M.; Schelz, Z.; Zupkó, I.; Csóka, I. Development of Lomustine and N-Propyl Gallate Co-Encapsulated Liposomes for Targeting Glioblastoma Multiforme via Intranasal Administration. *Pharmaceutics* **2022**, *14*, 631, doi:10.3390/pharmaceutics14030631.

94. Sipos, B.; Bella, Z.; Gróf, I.; Veszelka, S.; Deli, M.A.; Szűcs, K.F.; Sztojkov-Ivanov, A.; Ducza, E.; Gáspár, R.; Kecskeméti, G.; et al. Soluplus® Promotes Efficient Transport of Meloxicam to the Central Nervous System via Nasal Administration. *Int J Pharm* **2023**, *632*, 122594, doi:10.1016/j.ijpharm.2023.122594.

95. Abdullah, G.; Abdulkarim, M.; Salman, I.; Ameer, O.Z.; Yam, M.F.; Mutee; Chitneni; Mahdi, E.S.; Basri; Sattar, M.; et al. In Vitro Permeation and in Vivo Anti-Inflammatory and Analgesic Properties of Nanoscaled Emulsions Containing Ibuprofen for Topical Delivery. *IJN* **2011**, 387, doi:10.2147/IJN.S14667.

96. Saengkrit, N.; Saesoo, S.; Woramongkolchai, N.; Sajomsang, W.; Phunpee, S.; Dharakul, T.; Ruktanonchai, U.R. Dry Formulations Enhanced Mucoadhesive Properties and Reduced Cold Chain Handing of Influenza Vaccines. *AAPS PharmSciTech* **2018**, *19*, 3763–3769, doi:10.1208/s12249-018-1181-2.

97. Mosmann, T. Rapid Colorimetric Assay for Cellular Growth and Survival: Application to Proliferation and Cytotoxicity Assays. *J Immunol Methods* **1983**, *65*, 55–63, doi:10.1016/0022-1759(83)90303-4.

98. Raj, A.; Thomas, R.K.; Vidya, L.; Aparna, V.M.; Neelima, S.; Sudarsanakumar, C. Exploring the Cytotoxicity on Human Lung Cancer Cells and DNA Binding Stratagem of Camptothecin Functionalised Silver Nanoparticles through Multi-Spectroscopic, and Calorimetric Approach. *Sci Rep* **2023**, *13*, 9045, doi:10.1038/s41598-023-34997-w.

99. Rekha, S.; Anila, E.I. In Vitro Cytotoxicity Studies of Surface Modified CaS Nanoparticles on L929 Cell Lines Using MTT Assay. *Mater Lett* **2019**, *236*, 637–639, doi:10.1016/j.matlet.2018.11.009.

100. Hubatsch, I.; Ragnarsson, E.G.E.; Artursson, P. Determination of Drug Permeability and Prediction of Drug Absorption in Caco-2 Monolayers. *Nat Protoc* **2007**, *2*, 2111–2119, doi:10.1038/nprot.2007.303.

101. Katona, G.; Sipos, B.; Budai-Szűcs, M.; Balogh, G.T.; Veszelka, S.; Gróf, I.; Deli, M.A.; Volk, B.; Szabó-Révész, P.; Csóka, I. Development of In Situ Gelling Meloxicam-Human Serum Albumin Nanoparticle Formulation for Nose-to-Brain Application. *Pharmaceutics* **2021**, *13*, 646, doi:10.3390/pharmaceutics13050646.

102. Jespersen, B.; Knupp, L.; Northcott, C.A. Femoral Arterial and Venous Catheterization for Blood Sampling, Drug Administration and Conscious Blood Pressure and Heart Rate Measurements. *JoVE* **2012**, 3496, doi:10.3791/3496.

103. Jain, R.; Jain, B.; Kabir, A.; Bajaj, A.; Ch, R.; Sharma, S. Fabric Phase Sorptive Extraction-Gas Chromatography-Mass Spectrometry for the Determination of Favipiravir in Biological and Forensic Samples. *Advances in Sample Preparation* **2023**, *6*, 100058, doi:10.1016/j.sampre.2023.100058.

104. Zhang, Y.; Huo, M.; Zhou, J.; Xie, S. PKSolver: An Add-in Program for Pharmacokinetic and Pharmacodynamic Data Analysis in Microsoft Excel. *Comput Methods Programs Biomed* **2010**, *99*, 306–314, doi:10.1016/J.CMPB.2010.01.007.

105. Abou-Taleb, H.A.; Khallaf, R.A.; Abdel-Aleem, J.A. Intranasal Niosomes of Nefopam with Improved Bioavailability: Preparation, Optimization, and in-Vivo Evaluation. *Drug Des Devel Ther* **2018**, *12*, 3501, doi:10.2147/DDDT.S177746.

106. Ahmed, T.A. Preparation of Finasteride Capsules-Loaded Drug Nanoparticles: Formulation, Optimization, in Vitro, and Pharmacokinetic Evaluation. *Int J Nanomedicine* **2016**, *11*, 515–527, doi:10.2147/IJN.S98080.

107. Ibrahim, M.M.; Basalious, E.B.; El-Nabarawi, M.A.; Makhlouf, A.I.A.; Sayyed, M.E.; Ibrahim, I.T. Nose to Brain Delivery of Mirtazapine via Lipid Nanocapsules: Preparation, Statistical Optimization, Radiolabeling, in Vivo Biodistribution and Pharmacokinetic Study. *Drug Deliv Transl Res* **2024**, *14*, 2539–2557, doi:10.1007/S13346-024-01528-7.

108. Rompicherla, S.K.L.; Arumugam, K.; Bojja, S.L.; Kumar, N.; Rao, C.M. Pharmacokinetic and Pharmacodynamic Evaluation of Nasal Liposome and Nanoparticle Based Rivastigmine Formulations in Acute and Chronic Models of Alzheimer's Disease. *Naunyn Schmiedebergs Arch Pharmacol* **2021**, *394*, 1737–1755, doi:10.1007/S00210-021-02096-0/FIGURES/13.

109. Bhandari, R.; Kaur, I.P. Pharmacokinetics, Tissue Distribution and Relative Bioavailability of Isoniazid-Solid Lipid Nanoparticles. *Int J Pharm* **2013**, *441*, 202–212, doi:10.1016/J.IJPHARM.2012.11.042.

110. Kohajda, Z.; Virág, L.; Hornyik, T.; Husti, Z.; Sztojkov-Ivanov, A.; Nagy, N.; Horváth, A.; Varga, R.; Prorok, J.; Szlovák, J.; et al. In Vivo and Cellular Antiarrhythmic and Cardiac Electrophysiological Effects of Desethylamiodarone in Dog Cardiac Preparations. *Br J Pharmacol* **2022**, *179*, 3382–3402, doi:10.1111/BPH.15812.

111. Akel, H.; Ismail, R.; Katona, G.; Sabir, F.; Ambrus, R.; Csóka, I. A Comparison Study of Lipid and Polymeric Nanoparticles in the Nasal Delivery of Meloxicam: Formulation, Characterization, and in Vitro Evaluation. *Int J Pharm* **2021**, *604*, 120724, doi:10.1016/J.IJPHARM.2021.120724.

112. D'Souza, S.; Faraj, J.A.; Giovagnoli, S.; DeLuca, P.P. IVIVC from Long Acting Olanzapine Microspheres. *Int J Biomater* **2014**, *2014*, 1–11, doi:10.1155/2014/407065.

113. Sipos, B.; Szabó-Révész, P.; Csóka, I.; Pallagi, E.; Dobó, D.G.; Bélteky, P.; Kónya, Z.; Deák, Á.; Janovák, L.; Katona, G. Quality by Design Based Formulation Study of Meloxicam-Loaded Polymeric Micelles for Intranasal Administration. *Pharmaceutics* **2020**, *12*, 1–29, doi:10.3390/PHARMACEUTICS12080697.

114. Bansal, A.; Kapoor, D.; Kapil, R.; Chhabra, N.; Dhawan, S. Design and Development of Paclitaxel-Loaded Bovine Serum Albumin Nanoparticles for Brain Targeting. *Acta Pharmaceutica* **2011**, *61*, 141–156, doi:10.2478/v10007-011-0012-8.

115. Lohcharoenkal, W.; Wang, L.; Chen, Y.C.; Rojanasakul, Y. Protein Nanoparticles as Drug Delivery Carriers for Cancer Therapy. *Biomed Res Int* **2014**, *2014*, 1–12, doi:10.1155/2014/180549.

116. Galisteo-González, F.; Molina-Bolívar, J.A. Systematic Study on the Preparation of BSA Nanoparticles. *Colloids Surf B Biointerfaces* **2014**, *123*, 286–292, doi:10.1016/j.colsurfb.2014.09.028.

117. Masserini, M. Nanoparticles for Brain Drug Delivery. *ISRN Biochem* **2013**, *2013*, 1–18, doi:10.1155/2013/238428.

118. Naman, S.; Madhavi, N.; Singh, B.; Madan, J.; Baldi, A. Implementing Risk-Based Quality by Design for Development and Optimization of Flavored Oral Disintegrating Mini Tablets. *J Drug Deliv Sci Technol* **2021**, *66*, 102799, doi:10.1016/j.jddst.2021.102799.

119. Sailaja, A.K.; Vineela, C. Preparation and Characterization of Mefenamic Acid Loaded Bovine Serum Albumin Nanoparticles by Desolvation Technique Using Acetone as Desolvating Agent. **2014**.

120. Maghsoudi, A.; Shojaosadati, S.A.; Vasheghani Farahani, E. 5-Fluorouracil-Loaded BSA Nanoparticles: Formulation Optimization and In Vitro Release Study. *AAPS PharmSciTech* **2008**, *9*, 1092–1096, doi:10.1208/s12249-008-9146-5.

121. Hoseini, B.; Jaafari, M.R.; Golabpour, A.; Momtazi-Borojeni, A.A.; Karimi, M.; Eslami, S. Application of Ensemble Machine Learning Approach to Assess the Factors Affecting Size and Polydispersity Index of Liposomal Nanoparticles. *Sci Rep* **2023**, *13*, 18012, doi:10.1038/s41598-023-43689-4.

122. Neves, A.R.; Queiroz, J.F.; Reis, S. Brain-Targeted Delivery of Resveratrol Using Solid Lipid Nanoparticles Functionalized with Apolipoprotein E. *J Nanobiotechnol* **2016**, *14*, 27, doi:10.1186/s12951-016-0177-x.

123. Kalidasan, V.; Liu, X.L.; Herng, T.S.; Yang, Y.; Ding, J. Bovine Serum Albumin-Conjugated Ferrimagnetic Iron Oxide Nanoparticles to Enhance the Biocompatibility and Magnetic Hyperthermia Performance. *Nano-Micro Lett.* **2016**, *8*, 80–93, doi:10.1007/s40820-015-0065-1.

124. Mohanraj, K.; Sethuraman, S.; Krishnan, U.M. Development of Poly(Butylene Succinate) Microspheres for Delivery of Levodopa in the Treatment of Parkinson's Disease. *J Biomed Mater Res* **2013**, *101B*, 840–847, doi:10.1002/jbm.b.32888.

125. Ahmed, L.; Atif, R.; Eldeen, T.S.; Yahya, I.; Omara, A.; Eltayeb, M. Study the Using of Nanoparticles as Drug Delivery System Based on Mathematical Models for Controlled Release. **2019**.

126. Wiltschko, L.; Roblegg, E.; Raml, R.; Birngruber, T. Small Volume Rapid Equilibrium Dialysis (RED) Measures Effects of Interstitial Parameters on the Protein-Bound Fraction of Topical Drugs. *J Pharm Biomed Anal* **2023**, *234*, 115571, doi:10.1016/J.JPBA.2023.115571.

127. Salade, L.; Wauthoz, N.; Goole, J.; Amighi, K. How to Characterize a Nasal Product. The State of the Art of in Vitro and Ex Vivo Specific Methods. *Int J Pharm* **2019**, *561*, 47–65, doi:10.1016/j.ijpharm.2019.02.026.

128. Cannella, V.; Altomare, R.; Chiaramonte, G.; Di Bella, S.; Mira, F.; Russotto, L.; Pisano, P.; Guercio, A. Cytotoxicity Evaluation of Endodontic Pins on L929 Cell Line. *Biomed Res Int* **2019**, *2019*, 1–5, doi:10.1155/2019/3469525.

129. Shankar Raman, S.; Narayanan, V.H.B.; Durai, R. Lamotrigine Nanoparticle Laden Polymer Composite Oral Dissolving Films for Improving Therapeutic Potential of the Hydrophobic Antiepileptic Molecule. *Assay Drug Dev Technol* **2021**, *19*, 2–16, doi:10.1089/adt.2020.992.

130. Marcello, E.; Chiono, V. Biomaterials-Enhanced Intranasal Delivery of Drugs as a Direct Route for Brain Targeting. *IJMS* **2023**, *24*, 3390, doi:10.3390/ijms24043390.

131. Samaridou, E.; Alonso, M.J. Nose-to-Brain Peptide Delivery – The Potential of Nanotechnology. *Bioorg Med Chem* **2018**, *26*, 2888–2905, doi:10.1016/j.bmc.2017.11.001.

132. Aboul-Einien, M.H.; Kandil, S.M.; Abdou, E.M.; Diab, H.M.; Zaki, M.S.E. Ascorbic Acid Derivative-Loaded Modified Aspasomes: Formulation, in Vitro, Ex Vivo and Clinical Evaluation for Melasma Treatment. *J Liposome Res* **2020**, *30*, 54–67, doi:10.1080/08982104.2019.1585448.

133. d'Avanzo, N.; Cristiano, M.C.; Di Marzio, L.; Bruno, M.C.; Paolino, D.; Celia, C.; Fresta, M. Multidrug Idebenone/Naproxen Co-loaded Aspasomes for Significant in Vivo Anti-inflammatory Activity. *ChemMedChem* **2022**, *17*, doi:10.1002/cmdc.202200067.

134. Honary, S.; Zahir, F. Effect of Process Factors on the Properties of Doxycycline Nanovesicles. *Tropical Journal of Pharmaceutical Research* **2012**, *11*, 169–175, doi:10.4314/TJPR.V11I2.1.

135. Tangri, P.; Khurana, S. NIOSOMES: FORMULATION AND EVALUATION. 7.

136. Danaei, M.; Dehghankhold, M.; Ataei, S.; Hasanzadeh Davarani, F.; Javanmard, R.; Dokhani, A.; Khorasani, S.; Mozafari, M.R. Impact of Particle Size and Polydispersity Index on the Clinical Applications of Lipidic Nanocarrier Systems. *Pharmaceutics* **2018**, *10*, 57, doi:10.3390/pharmaceutics10020057.

137. Zolghadri, S.; Asad, A.G.; Farzi, F.; Ghajarzadeh, F.; Habibi, Z.; Rahban, M.; Zolghadri, S.; Stanek, A. Span 60/Cholesterol Niosomal Formulation as a Suitable Vehicle for Gallic Acid Delivery with Potent In Vitro Antibacterial, Antimelanoma, and Anti-Tyrosinase Activity. *Pharmaceuticals* **2023**, *16*, 1680, doi:10.3390/ph16121680.

138. Imran, M.; Titilayo, B.; Adil, M.; Liyan-Zhang; Mehmood, Q.; Mustafa, S.H.; Shen, Q. Ascorbyl Palmitate: A Comprehensive Review on Its Characteristics, Synthesis, Encapsulation and Applications. *Process Biochemistry* **2024**, *142*, 68–80, doi:10.1016/J.PROCBIO.2024.04.015.

139. Ekenna, I.C.; Abali, S.O. Comparison of the Use of Kinetic Model Plots and DD Solver Software to Evaluate the Drug Release from Griseofulvin Tablets. *Journal of Drug Delivery and Therapeutics* **2022**, *12*, 5–13, doi:10.22270/JDDT.V12I2-S.5402.

140. Jüptner, A.; Scherließ, R. Investigation of Powder Properties and Application Aspects Impacting Nasal Deposition of Spray-Dried Powders in a Nasal Cast. **2025**, doi:10.1016/j.ejpb.2025.114666.

141. Doub, W.H.; Suman, J.M.; Copley, M.; Goodey, A.P.; Hosseini, S.; Mitchell, J.P. Laboratory Performance Testing of Aqueous Nasal Inhalation Products for Droplet/Particle Size Distribution: An Assessment from the International Pharmaceutical Aerosol Consortium on Regulation and Science (IPAC-RS). *AAPS PharmSciTech* **2023**, *24*, 1–13, doi:10.1208/S12249-023-02665-X/TABLES/4.

142. Patterlini, V.; Guareschi, F.; D'Angelo, D.; Baldini, S.; Meto, S.; Mostafa Kamal, D.; Fabrizzi, P.; Buttini, F.; Mösges, R.; Sonvico, F. Clinically Relevant Characterization and Comparison of Ryaltris and Other Anti-Allergic Nasal Sprays. *Pharmaceutics* **2024**, *16*, doi:10.3390/PHARMACEUTICS16080989/S1.

143. Abourehab, M.A.S.; Khames, A.; Genedy, S.; Mostafa, S.; Khaleel, M.A.; Omar, M.M.; El Sisi, A.M. Sesame Oil-Based Nanostructured Lipid Carriers of Nicergoline, Intranasal Delivery System for Brain Targeting of Synergistic Cerebrovascular Protection. *Pharmaceutics* **2021**, *13*, 581, doi:10.3390/pharmaceutics13040581.

144. Basiri, L.; Rajabzadeh, G.; Bostan, A. Physicochemical Properties and Release Behavior of Span 60/Tween 60 Niosomes as Vehicle for α-Tocopherol Delivery. *LWT* **2017**, *84*, 471–478, doi:10.1016/j.lwt.2017.06.009.

145. Rong, J.; Zhao, C.; Xia, X.; Li, G.; Haider, A.; Wei, H.; Chen, J.; Xiao, Z.; Li, Y.; Zhou, X.; et al. Evaluation of [18F]Favipiravir in Rodents and Nonhuman Primates (NHP) with Positron Emission Tomography. *Pharmaceuticals* **2023**, *16*, 524, doi:10.3390/ph16040524.

146. Formica, M.L.; Real, D.A.; Picchio, M.L.; Catlin, E.; Donnelly, R.F.; Paredes, A.J. On a Highway to the Brain: A Review on Nose-to-Brain Drug Delivery Using Nanoparticles. *Appl Mater Today* **2022**, *29*, 101631, doi:10.1016/J.APMT.2022.101631.